이학박사학위논문

Neuropathic pain gene-expression signatures in spinal microglia following nerve injury via near single-cell transcriptome analysis

고해상도 전사체 분석법을 통한 신경손상 후 척수 소교세포의 신경병증성 통증 유전자 발현에 관한 연구

2017년 8월

서울대학교 대학원

치의과학과 신경생물학 전공

정 희 진

ABSTRACT

Neuropathic pain gene-expression signatures in spinal microglia following nerve injury via near single-cell transcriptome analysis

Heejin Jeong
Department of Dental Science, Program in Neuroscience
The Graduate School
Seoul National University

Microglia are resident immune cells responsible for maintaining homeostasis and sensing neuronal injury in the central nervous system (CNS). Microglial activation in response to peripheral nerve injury is known to be important in inducing pain hypersensitivities. Activated microglia is accompanied by changes in hypertrophic morphology, rate of proliferation, and alterations in gene expression. Large-scale screening to identify pain-related genes on tissue level such as in dorsal root ganglion (DRG) and spinal cord has revealed significantly altered expression of a number of genes. However, most of these genes are neuronal not microglial, indicating that whole tissue analysis may have limitations in finding targets from

minor fraction of whole tissue transcriptome.

In the present study, I adopted high resolution transcriptome assay from individually collected pools of 10 spinal microglia cells to identify changes in expression levels and cell-to-cell variation of activated microglial genes in peripheral nerve injury model. Differentially expressed genes (DEGs) analysis revealed that miR-29c was a critical factor for microglia activation and the development of neuropathic pain at post-operative day 1 (POD1). According to gene ontology analysis, early POD1 microglia exhibited a very distinct expression profile compared to late POD7 microglia, possibly leading to the transition from initiation to maintenance of neuropathic pain. Genes related to sensing function were influenced at POD1 while expressions of genes induced by signaling pathways were more predominant at POD7. Variation analysis revealed that 56 genes in group C genes showed decreased variance in injury with concomitant increase in variance in sham. In fact, only the group C genes showed tight clustering of the four experimental conditions. The 56 microglial genes, including Gria1, the gene encoding AMPA receptor subunit GluA1, potentially linked to the maintenance of neuropathic pain. Gria1 may regulate TNFα release via changing permeability of the AMPA receptor to Ca^{2+} influx. This study provides insights into spinal microglial

biology and reveals novel microglial targets for the treatment of neuropathic pain.

Key Words: Spinal microglia, High-resolution transcriptome, Neuropathic pain, MiR-29c, Gria1

Student Number: 2010-30656

CONTENTS

LIST OF FIGURES

BACKGROUND

1. Microglial activation

First introduced by Rio-Hortega, microglia are resident macrophages of the central nervous system (CNS) that form branched, ramified morphological phenotype in the physiological state (del Rı´o-Hortega 1919; Kettenmann et al. 2011; Mittelbronn et al. 2001). Microglia monitor and sense the various pathological changes of the CNS (Kreutzberg 1996; Nimmerjahn et al. 2005; Streit 2002). In the pathological conditions such as infection, trauma, ischemia and neurodegenerative disease, microglia undergo rapid and profound changes in morphology, gene expression and functional behavior, which are also termed microglia activation (Block et al. 2007; Graeber and Streit 2010). Activated microglia become amoeboid in appearance, proliferate and migrate toward injured areas, where they release many pro-inflammatory factors such as cytokines, chemokines and reactive oxygen species (ROS) that can affect neurons and astrocytes, changing their functions to be easily excitable (Hanisch and Kettenmann 2007; Streit et al. 1999). Activated microglia also express diverse cell surface molecules and inflammatory molecules such as c5a receptor (C5aR), major histocompatibility complex (MHC) class I and II,

and purinergic receptors and toll-like receptors (Abbadie 2005; Kim et al. 2007; Tanga et al. 2005).

2. Microglial activation in neuropathic pain

Neuropathic pain is the most severe form of chronic pain that occurs after nerve damage, such as that is induced by bone compression in cancer, diabetes, infection or physical injury. Sciatic nerve injury in rodents leads to persistent tactile allodynia in which innocuous stimuli elicits abnormal pain hypersensitivity and spontaneous pain, two main symptoms of neuropathic pain (Campbell and Meyer 2006). Neuropathic pain involves aberrant excitability of nervous system following nerve injury (Costigan et al. 2010). Interestingly, neuropathic pain is regulated by immune reactions in the spinal cord, which are mediated by resident microglia and astrocytes, as well as infiltrating immune cells (Grace et al. 2014; Mika et al. 2013; Ren and Dubner 2010). Indeed, it has been reported that microglia contribute to central sensitization (Ikeda et al. 2012; Raghavendra et al. 2003).

In response to peripheral nerve injury, spinal microglia become activated through a progressive series of cellular and molecular changes (Calvo and Bennett 2012; Hanisch and Kettenmann 2007). Activated microglia in spinal dorsal horns have pivotal roles in neuropathic pain

through involvement in the central sensitization, a key mechanism for the development of neuropathic pain (Hains and Waxman 2006; Inoue and Tsuda 2009; Scholz and Woolf 2007; Tsuda et al. 2005; Watkins et al. 2001). In pathophysiological conditions, microglia release various inflammatory mediators, such as IL-1β, TNFα, PGE2 and nitric oxide (Ramesh et al. 2013; Smith et al. 2012; Zhang and An 2007). Increased TNFα in DRG or spinal cord is associated with neuropathic pain by activation of p38 MAPK in primary sensory neurons (Schafers et al. 2002; Schafers et al. 2003). Previous studies revealed that antagonism of TNFα alleviate pain hypersensitivity (Sommer et al. 2001a; Sommer et al. 2001b). Indeed, some studies indicate that intrathecal administration of IL-1β or TNFα can lead to neuropathic pain in normal rats (Reeve et al. 2000; Sung et al. 2004).

Many studies have demonstrated that nerve injury phosphorylates p38 MAPK in spinal cord microglia (Ji and Suter 2007). Phosphorylated p38 levels are low in the spinal cord of non-injured rats. Nerve injury induces a substantial increase in pp38 levels in spinal cells expressing the microglial markers, CD11b and Iba1 (Jin et al. 2003; Tsuda et al. 2004). Tsuda *et al*. showed that the activation of microglia in neuropathy requires P2X4 receptors, which are upregulated and specifically expressed by microglia in neuropathic pain models (Tsuda et al. 2003). ATP released from

dorsal horn neurons of the spinal cord bind to P2X and P2Y receptors on microglia (Masuda et al. 2016). Activation of P2X4 receptor accompanies phosphorylation of p38, which increases the synthesis and release of brain-derived neurotrophic factor (BDNF) in microglia (Coull et al. 2005). BDNF suppress inhibitory synaptic transmission in the spinal cord that augments neuropathic pain. In addition, an antibiotic minocycline, an inhibitor of microglia activity, attenuated predominately the development of tactile allodynia in animals (Raghavendra et al. 2003).

Despite recent progress in our understanding of microglia biology (Butovsky et al. 2014; Chiu et al. 2013; Hickman et al. 2013) and identification of several microglial factors which contribute to neuropathic pain (Clark et al. 2007; Tsuda et al. 2003; Ulmann et al. 2008), the molecular mechanisms by which resting microglia transform into activated microglia after nerve injury have not yet been fully elucidated.

3. Gene expression in neuropathic pain

Cellular phenotypes are determined by various processes involving gene and protein expression (Yang et al. 2004). In an attempt to reveal factors important for microglial activation and to understand microglial biology microglial activation factor and understand microglial biology, a

recent study has profiled global gene expression changes using resting and activated microglial cells from the rat brain (Parakalan et al. 2012). A number of studies carried out microarray analysis to identify novel pain-related factors (Costigan et al. 2010; Strong et al. 2012). Large-scale screening for pain-related genes on spinal cord or dorsal root ganglia (DRG) has revealed substantial expressional changes in hundreds of genes (Costigan et al. 2010; Lacroix-Fralish et al. 2006). Vicuna *et al*. found a novel pain gene, Serpin A3N, a serine protease inhibitor, through large-scale transcriptome profiling (Vicuna et al. 2015). Mice lacking Serpin A3N showed more neuropathic pain hypersensitivity than wild-type (WT) mice, and exogenous treatment of SerpinA3N tempered mechanical allodynia in WT mice (Vicuna et al. 2015). However, most of these genes revealed by large-scale screening are neuronal not microglial genes, indicating that whole tissue analysis may have limitations in finding targets from the spinal microglia whose transcriptome is expected to be a minor fraction of whole tissue transcriptome.

To overcome these limitations, high-throughput screening of single-cells has been considered. Single-cell transcriptome analysis has revealed cell-to-cell variations from the same tissue, which were masked at the whole tissue level (Eberwine et al. 2014; Sandberg 2014). Recently, Sandberg

suggested that a study on grouping and functioning of cells in an unbiased way using biological differences between single-cells will be needed (Sandberg 2014). Interestingly, a recent study showed the classification of sensory neurons that respond to sensory types by using unbiased classification of DRGs using single-cell RNA sequencing (Usoskin et al. 2015). Growing body of evidence revealed that there is transcriptome variation across individual cells of the same cell type (Chiu et al. 2014; Poulin et al. 2014). Dueck et al has reported that cell-to-cell heterogeneity may be important for higher-level function (Dueck et al. 2016). This suggests that high-resolution analysis at single-cell level may provide new information concerning the specific microglial genes involved in the activation of microglia in neuropathic pain.

PURPOSE

Molecular and cellular changes caused by peripheral nerve injury in the nervous system contribute to initiation of neuropathic pain. In particular, activation of microglia plays a critical role in the development of neuropathic pain. However, the molecular mechanism underlying microglia activation has not yet been elucidated. In this thesis study, I employed high-resolution single-cell microarray analysis of microglia from spinal cord slices after L4 spinal nerve transection to achieve following aims.

- To identify novel genes exclusively involved in microglia activation after nerve injury which may lead to initiation of neuropathic pain.
- To find novel microglial genes specifically involved in the transition to maintenance of neuropathic pain.

INTRODUCTION

Chronic pain is one of the main public medical issues that undermine the quality of life, especially due to the current lack of effective therapies controlling pain in patients (Costigan et al. 2009; Dworkin et al. 2003). Neuropathic pain is the most difficult form of chronic pain, and sciatic nerve injury in rodents leads to persistent tactile allodynia in which innocuous stimuli elicits abnormal pain hypersensitivity and spontaneous pain, two main symptoms of neuropathic pain (Campbell and Meyer 2006). Interestingly, neuropathic pain is regulated by immune reactions in the spinal cord, which are mediated by resident microglia and astrocytes, as well as infiltrating immune cells (Grace et al. 2014; Mika et al. 2013; Ren and Dubner 2010).

Microglia are resident immune cells of the central nervous system (CNS), participating both in maintaining homeostasis and in sensing pathological changes (Salter and Beggs 2014). In response to peripheral nerve injury, spinal microglia become activated following altered expression of multiple molecules, including cell surface receptors, intracellular signaling molecules, and secretary factors (Calvo and Bennett 2012; Hanisch and Kettenmann 2007). Activated microglia in spinal dorsal horns

contribute to central sensitization, the key mechanism for the development of neuropathic pain (Gao and Ji 2010; Hathway et al. 2009; Woolf 2011). Despite recent progress in our understanding of microglia biology (Butovsky et al. 2014; Chiu et al. 2013; Hickman et al. 2013) and identification of several microglial factors which contribute to neuropathic pain (Clark et al. 2007; Tsuda et al. 2003; Ulmann et al. 2008), the molecular mechanisms by which resting microglia are switched to activated forms after nerve injury have not yet fully understood. Given the poor efficacy of current drugs targeting neuronal activity in neuropathic pain (Grace et al. 2014), identifying microglial factors could be important for unraveling the molecular mechanisms and finding novel targets.

Cellular phenotypes are determined by multiple processes involving gene and protein expression (Yang et al. 2004). Large-scale screening for pain-related genes on spinal cord or DRG has revealed substantial expressional changes in hundreds of genes (Costigan et al. 2010; Lacroix-Fralish et al. 2006; Strong et al. 2012). However, most of these are neuronal, not microglial genes, indicating that whole tissue analysis may have limitations in finding targets from the spinal microglia whose transcriptome is expected to be a minor fraction of whole tissue transcriptome. Single-cell transcriptome analysis has revealed cell-to-cell variations from the same

tissue, which were masked at the whole tissue level (Eberwine et al. 2014; Sandberg 2014). These studies have suggested that an alternative approach for identifying microglial targets is to perform expression profiling at higher resolution, allowing us to identify rare transcripts and screen for effects on cell-to-cell variability.

In this study, I employed near single-cell microarray analysis of microglia from spinal cord slices following L4 spinal nerve transection (SNT). Recent works have achieved single-cell resolution whole transcriptome (Kolodziejczyk et al. 2015), but given the size of the microglia, I collected pools of 10 cells. While a collection of 10 cells is not at the level of single cells, mechanical selection of individual cells helped generate microglia enriched samples. Using this approach, I investigated murine microglial transcriptome between nerve-injured versus sham-operated microglia at POD1 and POD7. By comparing gene profiles between these two time points, I aimed to identify novel genes exclusively involved in microglia activation after nerve injury which may lead to initiation of neuropathic pain, and to find novel microglial genes specifically involved in the transition of neuropathic pain from development stage to its maintenance stage.

MATERIALS AND METHODS

Mice

Adult C57BL/6 and heterozygous Cx3cr1$^{+/GFP}$ male mice (8-10 weeks) produced by breeding Cx3cr1$^{GFP/GFP}$ mice (Jung et al. 2000) to wild type C57BL/6 were used in this study. Five mice per cage were kept. All animals were housed on a 12h/12h light/dark cycle with food and water provided *ad libitum*. Mice were acclimatized for at least one week prior to experiments.

Animal model

All surgical and experimental procedures were reviewed and approved by the Institutional Animal Care and Use Committee (IACUC) of the School of Dentistry, Seoul National University prior to the experiments. Animal treatments were performed according to the Guidelines of the International Association for the Study of Pain. For the spinal nerve transection model, the surgery was performed as described previously (DeLeo et al. 2000; Kim and Chung 1992). Under sodium pentobarbital anesthesia, a 1 cm longitudinal incision overlying the L3–L6 section was

made. The right paraspinal muscles were separated from the superior articular processes and the transverse processes to expose the L3 and L4 spinal nerves. The L4 spinal nerve was transected without damaging the L3 spinal nerve. The wound was closed by suturing the muscle and skin layers. Sham group received a sham surgery without nerve transection.

Behavioral test

Mechanical sensitivity was assessed at 1-day and 7-days after nerve injury during daytime by the up–down method using calibrated von Frey filaments as described previously (Chaplan et al. 1994). Six mice for each group were tested. Mice were acclimatized on a metal mesh floor (3 × 3 mm) in transparent plastic boxes (60 × 100 × 60 mm) for 1 hr. The mechanical sensitivity was evaluated using a set of eight calibrated von Frey filaments (0.02, 0.04, 0.07, 0.16, 0.4, 0.6, 1.0 and 1.4 g; Stoelting, Chicago, IL, USA) that were applied to the plantar surface of the hindpaw until the filament bent slightly for a few seconds. A withdrawal reflex of the hindpaw during stimulation or immediately after stimulus removal was considered a positive response. The first stimulus was always the 0.4 g filament. When there was a positive response, the next lower filament was applied, and when there was no response, the next higher filament was used. After the first change in

responses, four additional responses were observed, and the 50% paw withdrawal threshold value was calculated (Dixon 1980). Sensorymotor coordination was examined by rotarod test. All behavioral testing were performed blindly.

Microglial cell collection

Mice were deeply anesthetized with excess isoflurane and the spinal cord including lumbosacral enlargement was exposed by a dorsal laminectomy. Dissected tissue blocks were placed into ice-cold cutting solution containing (in mM): 245 sucrose; 3 KCl; 6.0 $MgCl_2$; 0.5 $CaCl_2$; 26 $NaHCO_3$; 1.25 NaH_2PO_4; 11 glucose; 5 HEPES; 1.0 Kynurenic acid (pH 7.4, when bubbled with 95% O_2/ 5% CO_2). Transverse slices (300 μm) were prepared using vibroslicer (Lieca VT1000 Plus, Leica Microsystems, Germany) and collected in a slice chamber containing recording artificial cerebrospinal fluid (aCSF) composed of (in mM): 126 NaCl; 3 KCl; 1.3 $MgCl_2$; 2.5 $CaCl_2$; 26 $NaHCO_3$; 1.25 NaH_2PO_4; 11 glucose; 5 HEPES (pH 7.4, when bubbled with 95% O_2 and 5% CO_2 and had osmolarity of 305 - 310 mOsmol). The slices were initially maintained at 32℃ for 45 min to recover and transferred to the slice chamber kept at room temperature (25 ± 1℃) until used. Individual cell collection was performed as previously

described (Kim et al. 2012). Cx3cr1-enhanced green fluorescent protein (EGFP)-positive microglia located in superficial dorsal horn was visualized under fluorescence microscopy and individual spinal microglia were collected with glass pipette, gently put into a reaction tube containing reverse transcription reagents. Individually identified microglia to form pure samples of 10 cells were used for each microarray transcriptome assay. Each sample represents an average of 10 cells and although the measurement is not at the single-cell level, the sample-to-sample variation is expected to be proportional to the single cell variation. If the variance of single cell is v, then the variance of the 10-cell averages is expected to be proportional to v/10. cDNA was synthesized from pooled ten microglia which were collected from three spinal cord slices of all from one animal and then used for each microarray chip. The ten microglia were selected six times for each experimental group which consists of six mice. A total of 24 mice were tested.

RNA isolation and microarray expression profiling

Microarray samples were prepared as described previously (Esumi et al. 2008). Briefly, the total RNA from ten pooled microglia was reverse-transcribed into cDNA using a SMARTer Pico PCR cDNA Synthesis Kit

(Takara Clontech, Kyoto, Japan). Advantage2 Polymerase Mix (Takara Clontech) was used to amplify the whole cDNA according to the manufacturer's instructions. The reaction profile was 1 min at 95℃; 20 cycles of 5 s at 95℃, 5 s at 65℃, 6 min at 68℃. I then added 2 μl of 12 μM modified primer II A with the T7 promoter and 2 μl of 50x Advantage2 Polymerase Mix again, and performed another thermal cycling for 1 min at 95℃; 10 cycles of 5 s at 95℃, 5 s at 65℃, 6 min at 68℃; 6 min at 68℃. To assess the quality of cDNA prepared from 10 pooled cells for microarray experiment, a portion of the cDNA (1 μl) was used as a template for nested PCR to detect β-actin and CD11b expression. Aspirated bath solution was used for the negative control. All PCR amplifications were performed with nested primers. The sequence used are as follows: CD11b, 5'-ACATGTGAG CCCCATAAAGC-3' and 5'-TCAGGGCTTCAAAGTTGTCC-3' in the first PCR (326 bp), 5'-ACATGTGAGCCCCATAAAGC-3' and 5'-AATGACCCCTGCTCTGTCTG-3' in the second nested PCR (205 bp); β-actin, 5'-CATCACTATTGGCAACGAGCG-3' and 5'-ACATCTGCTGGAAGGTGGACAG-3' in the first PCR (325 bp), 5'-GGCTCTTTTCCAGCCTTCCTT-3' and 5'-CCACCGATCCACACAGAGTACT-3' in the second nested PCR (251 bp).

With samples verified with RT-PCR, 3.4 μg per cDNA sample were used as input into the Affymetrix procedure as recommended by protocol. Amplified RNA (cRNA) was generated from the double-stranded cDNA template though an in-vitro transcription (IVT) reaction and purified with the Affymetrix sample cleanup module. cDNA was regenerated through a random-primed reverse transcription using a dNTP mix containing dUTP. The cDNA was then fragmented by uracil-DNA glycosylase (UDG) and apyrimidinic/apurinic endonuclease 1 (APE1) restriction endonucleases and end-labeled by terminal transferase reaction incorporating a biotinylated dideoxynucleotide. Fragmented end-labeled cDNA was hybridized to the Affymetrix GeneChip® Mouse Gene 1.0 ST arrays for 16 hours at 45℃ and 60 rpm as described in the Gene Chip Whole Transcript (WT) Sense Target Labeling Assay Manual (Affymetrix, Santa Clara, CA, USA). After hybridization, the chips were stained and washed in a Genechip Fluidics Station 450 (Affymetrix) and scanned by using a Genechip Array scanner 3000 7G (Affymetrix). Six biologically independent hybridizations were performed for each condition. The raw data for individual plates (libraries) are accessible (GEO: GSE60670).

Microarray data processing

The image data was extracted through Affymetrix Command Console software 1.1. The raw data (.cel files) generated through above procedure represented expression intensity data and was used for the next step. Expression data were generated by Affymetrix Expression Console software version1.1. Global gene expression profiles and single cell variation analysis were performed. Six biologically independent hybridizations were performed for each experimental group excluding sham POD1 group (n=5 for sham POD1 group). I excluded one of 'sham POD1' sample from the six 'sham POD1' samples since it was turned out that the sham POD1 sample was outlier according to the spearman's correlation coefficients analysis.

I normalized the arrays using Robust Multichip Average (RMA) normalization (Irizarry et al. 2003). In order to obtain robust expression values from 10-cell samples, I summarized perfect match (PM) probes on the array by specifically taking the log of the second highest PM probe intensity. In addition, I removed batch effects using a two-stage least squares method for estimation of location and scale parameters because non-biological variability such as differences in sample preparation and hybridization protocols can be potentially confounding biological differences (Giordan 2013). For differential expression analysis, t-test was

performed. To compare the distribution of CV between conditions, Wilcoxon rank-sum test was conducted. When I examined the distribution of CV of POD1 vs POD7 as well as Sham POD1 vs Sham POD7, both comparisons were significant at $p < 0.0001$ over the CV distribution of all the genes (20,694 genes). For heat maps, I used following web site; http://www.tm4.org/mev.html.

Metric multidimensional scaling (MDS) was performed to visualize the heterogeneity of gene expression profile between any pair of samples. Briefly, metric MDS finds an orthogonal projection to a set of axes ordered by the amount of variance. Additionally I applied linear discriminant analysis (LDA) to investigate whether different classes have distinct patterns where the axes were rescaled to make the two sets of projects comparable. LDA finds a linear function of the variables that maximizes the ratio of between-class variance and minimizes the ratio of within-class variance. MDS and LDA were carried out using an implementation in the R Statistical Software package downloaded from www.r-project.org.

To assess within-group similarity of gene expression, I used the symmetric Jensen-Shannon divergence (JSD) index, which ranges from 0 (identical) to 1 (‘distant’ distributions) such that lower JSD scores reflect higher similarity between transcriptomes. To measure cell-to-cell variability

captured in 10-cell units I used the coefficient of variation (CV) defined by the ratio of the standard deviation to the mean (CV = SD/mean). The variances between groups were assessed using an equality of variances F-test. A two sample F-test was performed to compare two population variances.

Functional and pathway analysis

To understand molecular functions involved in the early and late microglia respectively, each of the POD1-specific, POD7-specific, and common DEGs were input to Pathway Studio® (v 9.0, Ariadne Genomics, Rockville, MD, USA) (Nikitin et al. 2003) and GO classification was performed. Gene set enrichment analysis was applied to search for groups of genes involved in the same processes (gene sets) that were altered significantly by nerve injury. Cutoff parameters for significance were p-value < 0.01 and overlap (the number of overlapped genes) > 2. I analyzed disease pathways using Pathway Studio® . Disease entities were identified using the "common targets" option.

Primary microglia culture

Mixed glial cultures were prepared from cerebral cortex of 1-2 days old postnatal mice in accordance with the method described previously (Berta et al. 2014). After anesthetized, cerebral hemispheres were isolated and meninges were carefully removed. Tissues were then minced, triturated, filtered through a 100 μm nylon screen, and collected by centrifugation (3000g for 5 min). The cell pellets were broken with a pipette and resuspended in a medium containing 10 % fetal bovine serum in high glucose DMEM. After trituration, the cells were filtered through a 10 μm screen and grown on T75 flasks. Mixed glial cells were obtained from cultured and maintained for 14-16 days in high-glucose DMEM medium including 10% fetal bovine serum. Microglia were harvested from the mixed glia by shaking T75 flasks. The media including floating cells were collected and microglia were plated at 6-well plates at the density of 1.0 x 10^6 cells/ml for subsequent ATP treatments or used for transfection. Microglia purity was greater than 95%, as confirmed by Iba1 staining. After 2 days after plating, microglia were treated with 50 μM ATP (Sigma, St. Louis, MO, USA) for 1 hr which was previously shown to activate microglia (Tsuda et al. 2003).

Quantitative real-time RT-PCR

Total RNA or specifically the small RNA fraction was extracted by RNeasy mini kit and miRNeasy Mini kit (Qiagen, Valencia, CA, USA) respectively, and 0.5 - 1.0 μg was processed for cDNA synthesis using M-MLV Reverse Transcriptase (Invitrogen, Carlsbad, CA, USA) or miScript PCR Starter Kit (Qiagen) according to the manufacturer's instructions. The primers used for miRNA were as follows: miR-29b-3p, 5'-UAGCACCAUUUGAAAUCAGUGUU -3' (cat no. MS00005936, miScript Primer Assays); miR-29c-3p, 5'- UAGCACCAUUUGAAAUCGGUUA -3' (cat no. MS00001379, miScript Primer Assays); miR-137-3p, 5'-UUAUUGCUUAAGAAUACGCGUAG -3' (cat no. MS00001589, miScript Primer Assays); snRNA RNU6B (RNU6-2), which were provided in miScript PCR Starter Kit (cat no. MS00033740, miScript Primer Assays). Real-time PCR was performed with cDNA prepared for microarray experiment or obtained from primary cultured microglia as a template using a 7500 Real-Time PCR system (Applied Biosystems, Foster City, CA, USA). The threshold cycle (Ct) of the GAPDH or snRNA RNU6B was used as a reference control to normalize the expression level of the target gene (ΔCt) to correct for experimental variation. Relative mRNA levels were calculated according to the 2-ΔΔCt method (Livak and Schmittgen 2001). Real-time RT-PCR experiments were performed at least three times. Values

are presented as means ± SEM unless otherwise noted. The PCR primer sequences used in this study are as follows; GAPDH, 5'-TCCATGACAACTTTGGCATTG-3' and 5'-CAGTCTTCTGGGTGGCAGTGA-3'; Il-1β, 5'-ACCTGCTGGTGTGTGACGTTC-3' and 5'-CAGCACGAGGCTTTTTTGTTGT-3'; Tnfα, 5'- AGC AAA ECA CCA AGT GGA GGA-3' and 5'- GCT GGC ACCACTAGTTGGTTGT-3'; Cx3cr1, 5'-CAGCATCGACCGGTACCTT-3' and 5'-GCTGCACTGTCCGGTTGTT-3'; P2rx4, 5'-TGGCCGACTATGTGGTCCCA-3' and 5'-GGTTCACGGTGACGATCATG-3'; C5ar1, 5'-GTCCTGTTCACGACCGTTTT-3' and 5'-ACGGTCGGCACTAATGGTAG-3'; Hexb, 5'-AGCGCTGTTGGTGAGAGACT-3' and 5'-CTATTCCACGGCTGACCATT-3'; Gria1, 5'-TCAATGAAGCCATACGGACA-3' and 5'-GCTGACCACTCTGCCATTCT-3'; P2ry12, 5'-TTTGTTCCCTTCCACTTTGC-3' and 5'-AGGGTGCTCTCCTTCACGTA-3'; Glul, 5'-CTGCCATACCAACTTCAGCA-3' and 5'-

TGTGGTACTGGTGCCTCTTG-3’; Trf, 5’-CCGGGTTAAGGCTGTACTGA-3’ and 5’-ACAGAAGGTCCTTGGTGGTG-3’; Spg21, 5’-GAGTGCGCTGTCAACAGAAG-3’ and 5’-CTCCTGCACAGGTAGGGAAA-3’; Cdk5, 5’-GTCCATCGACATGTGGTCAG-3’ and 5’-GCTGGTCATCCACATCATTG-3’; Bank1, 5’-TTCAGCAGGAAAAGCTACGG-3’ and 5’-TGGTGCACAATGGTCAGTTT-3’; Arf6, 5’-CAGGGTCTGATCTTCGTGGT-3’ and 5’-CTCATCTCCCGGTCATTGAT-3’

Western blotting

Proteins were prepared using Pro-prep solution (Intron biotechnology, Kyunggi-do, Korea). Protein concentration was determined with BCA assay kit (Thermo Scientific, Rockford, IL, USA). 30 μg of proteins were separated by 10% SDS-PAGE electrophoresis and transferred onto PVDF membrane. After blocking, the membrane were probed with anti-phospho p38 (Cell Signaling, Danvers, MA, USA, cat.no.4631s, 1:1000) and anti-p38 (Cell Signaling, cat.no.9212, 1:1000) overnight followed by

horseradish peroxidase-conjugated anti-rabbit (Santa Cruz, Santa Cruz, CA, cat.no.sc2004, 1:5000) IgG for 1 hr at room temperature. Blots were detected and quantified using Gel-Doc XRS+ system (Bio-rad, Hercules, CA, USA) by chemiluminescent reagent (SuperSignal West Pico, Thermo Scientific, Rockford, IL, USA). Independent experiments were conducted at least three times.

Transfection

AccuTargetTM Gria1 siRNAs (1365968, Bioneer, Daejeon, Korea) and negative control siRNA were purchased from Bioneer. The antisense 2'-O-methyl (2'-O-Me) oligonucleotide for miR-29c inhibitor (2'-O-Me-29c-AS) and NC5 negative control were obtained from Integrated DNA Technologies (IDT, Coralville, IA, USA). The sequences of 2'-O-Me-29c-AS and NC5 negative control are 5'-mU/ZEN/mAmAmCmCmGmAmUmUmUmCmAmAmAmUmGmGmUmGmCmU/3ZEN-3' (r, RNA base; m, 2' O-methyl base) and 5'-mG/ZEN/mCmGmAmCmUmAmUmAmCmGmCmGmCmAmAmUmAmUmGmG/3ZEN-3' (r, RNA base; m, 2' O-methyl base). To increase miR-29c levels, we administered a chemically modified double-stranded miRNA mimic. Primary cultured microglia was transfected with Gria1 siRNA (10

nM) or miR-29c inhibitor (10 nM) or miR-29c mimic (10 nM) by electroporation using a microporatorTM (MP-100; Digital Bio Technology, Suwon, Korea) following the manufacturer's instructions. Transfected microglia was seeded at 1.0 x 10^6 cells per well of 6- well plates. Real-time PCR was used to determine knockdown efficacy of siRNA, miRNA inhibitor and miR-29c mimic. After 48 hr for Gria1 and miR-29c mimic, 60 hr for miR-29c inhibitor, we harvested the transfected microglia and, after centrifugation, transferred only microglial cell resuspended in PBS, without culture media, into animals.

Intrathecal injection and drug injection

Gria1-knockdown microglia or miR-29c -inhibited microglia (1.0 x 10^6 cells, 10 μl) were injected intrathecally in normal mice as described previously (Hylden and Wilcox 1980). Under isoflurane anesthesia, mice were injected using a 50 μl Hamilton syringe fitted with a 31 gauge needle by direct lumbar puncture between the L5 and L6 level. Control animals were injected with microglia transfected with NC5 negative control (miRNA inhibitor control, NC) or negative control siRNA (siScram). Paw withdrawal threshold was tested 1, 3 and 5 hr after injection.

TNFα antagonist etanercept (Enbrel; 25 mg/vial; Wyeth, Taplow, Maidenhead, UK) was administrated by systemic intraperitoneal injection 1 hr after microglial injection. Dilution before administrations was made in PBS for treatment of mice.

Preparation of DRG neurons

DRG neurons obtained from 4–6-week old mice were prepared. Animals were anesthetized with overdose of isoflurane, decapitated, and DRGs were rapidly removed under aseptic conditions and placed in HBSS (Gibco, Gaithersburg, Maryland, USA). DRGs were digested in 1 mg/ml collagenase A (Roche) and 2.4 U/ml dispase II (Roche) in HBSS for 60 min, respectively, followed by 8 min in 0.25% trypsin (Sigma), all at 37℃. The DRGs were then washed in Neurobasal medium (Gibco) three times and resuspended in DMEM medium supplemented with 10% FBS (Invitrogen) and 1% penicillin/streptomycin (Sigma). DRGs were then mechanically dissociated using fire polished glass pipettes, centrifuged (800 rpm, 5 min), resuspended in DMEM medium supplemented with 10% FBS (Invitrogen), 1X B-27 supplement (Invitrogen), 1× N-2 supplement (Invitrogen), and 1% penicillin/streptomycin (Invitrogen), and plated on 0.5 mg/ml poly-D-lysine

(Sigma)-coated glass coverslips. Cells were maintained at 37℃ in a 5% CO_2 incubator.

Ca^{2+} imaging

We performed fura-2 AM-based (Molecular Probes, Eugene, OR, USA) Ca^{2+} imaging experiments. DRG neurons were loaded with fura-2 AM (2 μM) for 40 min at 37°C in a balanced salt solution containing (in mM): 140 NaCl, 5 KCl, 2 $CaCl_2$, 1 $MgCl_2$, 10 N-[2-hydroxyethyl] piperazine-N′-[2-ethanesulfonic acid] (HEPES), 10 glucose, adjusted to pH 7.3 with NaOH. The cells were then rinsed with Neurobasal medium and incubated in Neurobasal medium for an additional 20 min to de-esterify the dye. Cells on slides were placed onto an inverted microscope and illuminated with a 175 W xenon arc lamp; excitation wavelengths (340/380 nm) were selected by a monochromator wavelength changer. Intracellular calcium concentrations ($[Ca^{2+}]_i$) were measured every 1 sec interval by digital video microfluorometry with an intensified charge-coupled-device camera (CasCade, Roper Scientific, Trenton, NJ, USA) coupled to the microscope and a computer with Metafluor software (Universal Imaging, Downingtown, PA, USA). Independent experiments were conducted at least three times.

Electrophysiology

Electrophysiological recordings of postsynaptic field potentials (fPSPs) evoked by dorsal root stimulation were made using a whole spinal cord preparation. Adult male C57BL/6 mice were anesthetized with excess isoflurane and the lumbar spinal column was removed and placed into ice-cold cutting solution containing (in mM): 245 sucrose; 3 KCl; 6.0 $MgCl_2$; 0.5 $CaCl_2$; 26 $NaHCO_3$; 1.25 NaH_2PO_4; 11 glucose; 5 HEPES; 1.0 Kynurenic acid (pH 7.4, when bubbled with 95% O_2/ 5% CO_2). After that the lumbar spinal cord was quickly removed via laminectomy and placed in aCSF composed of (in mM): 126 NaCl; 3 KCl; 1.3 $MgCl_2$; 2.5 $CaCl_2$; 26 $NaHCO_3$; 1.25 NaH_2PO_4; 11 glucose; 5 HEPES (pH 7.4, when bubbled with 95% O_2 and 5% CO_2 and had osmolarity of 305 - 310 mOsmol) for 1 hr before recordings. The fPSPs data were recorded and acquired using an EPC-10 amplifier (HEKA, Lambrecht, Germany) and Pulse 8.30 software (HEKA). fPSP recordings were performed at room temperature (23 ± 1℃) using ~ 3 MΩ borosilicate capillaries (World Precision Instruments, Sarasota, FL, USA) filled with aCSF. The electrodes were inserted into the dorsal side of the spinal cord in Lissauer's tract. Electrical stimuli (0.01 ms, 0.0167Hz) were delivered through a theta glass suction electrode, which was

filled with aCSF and placed in the dorsal root. After a baseline recording (10 min), the microglia (1 x 10^6 in 500 µl) were focally perfused into spinal dorsal horn through a borosilicate capillary placed toward the recording area. The amplitude of evoked fPSPs was measured, two consecutive fPSP were averaged, and these measurements were expressed relative to the normalized baseline.

Immunofluorescence

Following fixing microglia with 4% paraformaldehyde for 10 mins at room temperature, microglia were incubated for 1 hr in blocking solution containing 5% normal donkey serum (Jackson ImmunoResearch Laboratories, Bar Harbor, ME, USA) and 5% FBS (Gibco) in PBS-T (0.1% Triton X-100). The cells were incubated with primary antibody for rabbit anti-GluA1 (1: 500, Millipore, cat. no. AB1504) and rabbit anti Iba1 (1:1000, Wako, cat. no. 019-1974) at 4℃ overnight. After rinsing with PBS, the cells were incubated with Alexa fluor 488 goat anti-rabbit (1:200, Jackson ImmunoResearch Laboratories) and Cy3 fluor goat anti rabbit (1:200, Jackson ImmunoResearch Laboratories) at room temperature for 1 hr. Following washing with PBS, cells were mounted with vectashield mounting medium (Vector, Laboratories, Burlingame, CA, USA).

Fluorescent images were obtained using a confocal microscope (LSM700, Carl Zeiss, Jena, Germany). Independent experiments were performed at least three times.

Enzyme-linked immunosorbent assay (ELISA)

After transfection, primary cultured microglia were plated 1.5 x 10^6 cells/well in 6-well plates and cell supernatants were collected 48 hr after transfection. The level of TNFα in supernatants were quantified using the mouse TNFα Duoset ELISA kit (R&D Systems, Minneapolis, MN, USA, cat.no. DY410-05). For each reaction in a 96-well plate, 100 μl of supernatants was used, and ELISA was performed according to the manufacturer's instructions. Independent experiments were performed three times.

In situ hybridization of miR-29c

In situ hybridizations were performed in 14 μm cryosections from spinal cord. Sections were fixed in 4% paraformaldehyde-0.1 M PBS for 30 min followed by washes in DEPC-treated ultrapure water. After treatment with a mixture of 30% H_2O_2 and methanol (v/v=1:50) for 30 minutes, sections were treated with proteinase K (Boster, Wuhan, China) for 2 min at

room temperature. sections were prehybridized in hybridization solution (50% deionised formamide, 0.3 M NaCl, 5 mM EDTA, 10 mM $NaPO_4$, 0.5 mg/ml yeast tRNA, 10% Dextran Sulfate, 1×Denhardt's solution) at 25°C below the predicted Tm value of the LNA probe for 2 hr. Next, sections were incubated with 5'-DIG and 3'-DIG labeled mature miR-29c miRCURY LNA™ detection probe (/5DigN/TAA CCG ATT TCA AAT GGT GCT A/3Dig_N/) or microRNA Detection Control Probes for ISH (/5DigN/GTG TAA CAC GTC TAT ACG CCC A/3Dig_N/) (Exiqon, Vedbæk, Denmark) at 53℃ overnight. Sections were then incubated in blocking solution at 37℃ for 30 min and in mouse-anti-DIG-biotin for 60 min, washed, incubated using SABC-FITC regent (Boster) for 30 min. To identify the cell types expressing miR-29c, the above sections under ISH were incubated overnight at 4℃ with primary antibodies against GFAP (mouse, 1:6000, Millipore, Temecula, CA, USA), NeuN (mouse, 1:1000, Millipore) or IBA-1 (rabbit, 1:3000, Wako, Tokyo, Japan). On the following day, Cy3-conjugated secondary antibody was added and incubated for 2 hr. The signal was detected with a with a Leica fluorescence microscope, and images were captured with a CCD Spot camera.

Statistics

All data were checked for normality by Shapiro-Wilk test before statistical testing. For the data showing non-normal distribution, we performed Mann-Whitney U test. Data are presented as mean± SEM and were analyzed using SPSS and GraphPad Prism version 5.0 (GraphPad). For sample sizes, no statistical methods were used to predetermine sample sizes, but sample sizes used in this study are similar to those generally employed in this field. Statistical analyses of the 50% withdrawal thresholds were performed using Mann–Whitney U test at individual time points or two way repeated ANOVA. Unpaired two-tailed Student's *t*-test was used for real-time PCR analysis, western blotting and calcium imaging analysis. $p < 0.05$ was considered statistically significant.

RESULTS

Validation of 10-cell microarray data

L4 SNT produced significant mechanical allodynia from POD1 and peaked at POD7 (Fig. 1A). Microglia in the ipsilateral dorsal horn largely consisted of activated microglia, which was identified by Cx3cr1-EGFP-positive expression (Fig. 1B). I selected these two time points, POD1 and POD7 to compare microglia gene profiles during neuropathic pain initiation and development/maintenance against respective sham-operated controls (Fig. 1A). RT-PCR revealed the expression of CD11b (Fig. 1D) in microglia randomly collected with glass pipettes from superficial laminae of L3 – L5 spinal dorsal horn (Fig. 1C), but not in negative controls consisting of aspirates of the bath solution (Fig. 1D), indicating there was no detectable levels of RNA contamination.

To check the consistency of 10-cell microarray data, 14 microglial genes previously known to increase their expression after nerve injury and closely associated with neuropathic pain (Griffin et al. 2007; Tanga et al. 2005; Ulmann et al. 2008; Zhuang et al. 2007) were examined (Fig. 2A). Most of the 14 genes were up-regulated after injury. In contrast, housekeeping genes and most marker genes for other CNS cell types

showed insignificant changes (Fig. 2A, E). I further validated the data with real-time PCR by confirming increased expression of randomly selected five genes among the 14 microglial genes (Fig. 2D). I also examined 29 spinal cord microglia-specific genes recently reported by Chiu et al (Fig. 2B) (Chiu et al. 2013). I found 28 genes (except one gene missing on the microarray chip) highly expressed both in sham- and injured-microglia (Fig. 2B and Fig. 3A). Butovsky et al. reported 40 microglial genes uniquely expressed in central microglia but not in peripheral monocytes (Butovsky et al. 2014). These 40 genes were also expressed both in sham and injured microglia (Fig. 3B), and up-regulated following nerve injury compared with their respective sham controls (Fig. 2C, E). Taken together, these results demonstrate that the 14 previous known genes in 10-cell microarray results were consistent with expression profiles from previous studies and suitable for screening neuropathic pain-linked genes with minimal contamination from other CNS cell types.

Time-dependent differential changes in microglial gene expression after nerve injury

To find early and late responsive microglia genes to peripheral nerve injury, I determined differentially expressed genes (DEGs) by

comparing POD1 and POD7 with their respective sham-operated controls. A total of 559 genes whose expression significantly changed in microglia after nerve injury were identified. Of these, 312 genes were up-regulated and 247 genes were down-regulated (Fig. 4A). Of the 312 up-regulated genes, 123 were significantly up-regulated only at POD1 (POD1-specific DEG) and 167 were up-regulated only at POD7 (POD7-specific DEG). The overlap between POD1 and POD7 (common DEG) yielded 22 genes that were up-regulated throughout the course of pain (Fig. 4B). Interestingly, the POD1-specific DEGs included 3 miRNA genes: miR-137, miR-29b-1, miR-29c.

Next, I analyzed DEGs using Gene Ontology (GO) terms to assess whether certain functions or molecular pathways were significantly enriched within and across each time point. A number of genes related to chemotaxis, C5a signaling, succinate metabolic process, cytokine-mediated signaling, mitotic cell cycle, and cell shape were significantly enriched within the POD1 DEGs. For POD7, genes associated with Type I interferon-mediated signaling, cellular response to calcium ion, cytokine-mediated signaling, interferon-γ, chemotaxis and phospholipid metabolic process were significantly regulated (Fig. 4C). Gene functions involved in interleukin-6, chemokine, kinase, NF-κB, and toll-like receptor (TLR) signaling pathway were enriched in DEGs common to both time points (Fig. 4C). Interestingly,

early and late phase microglia were associated with distinct cellular compartments (Fig. 4D). Genes associated with membrane, mitochondrial matrix, and nucleus changed at POD1, whereas genes located in the trans-Golgi transport vesicle, cytosol and endoplasmic reticulum were largely altered at POD7. Plasma membrane-related genes were up-regulated throughout the course of pain (Fig. 4D). While GO analysis is often weak, these results suggest that Genes related to sensing function dominates at POD1 while expressions of genes induced by signaling pathways are more prevalent at POD7.

Identification of candidate pain-maintenance neuropathic microglial genes by variation analysis

I next investigated the sample-to-sample dispersion patterns to gain insights into potential single-cell variability of the microglia. The use of 10-cell samples is expected to reflect individual variability with a scaling factor of square root of sample number (n =10; see Methods). To visualize the dispersal patterns, metric multidimensional scaling (MDS) was carried out. Overall, POD7 and Sham POD7 were more dispersed than POD1 and Sham POD1, respectively (Fig. 5A). The two-dimensional projections of a subset of housekeeping genes (Fig. 5A, left) showed less dispersal than all genes in

the spinal microglia (Fig. 5A, right), suggesting that not all genes show broad variation (Fig. 6C). The Jensen-Shannon Divergence index was used to numerically quantify the visual pattern of variability (Fig 5B). As seen in Fig. 5B, for both sham and injury conditions, I observed a general increase in variability over the seven day period (Fig. 6A). Furthermore, I compared the ratio of variances of each gene (POD7/POD1 and Sham POD7/Sham POD1) by an F-test which showed that in the injury condition, a smaller number of genes increased in variation over time than in the sham condition (Fig. 6B). I note that unlike tissue samples with millions of cells that might average across minor (but with large changes in gene expression) cell subtypes, the altered transcriptome of our 10-cell sample collection might be disproportionately influenced by these few cell subtypes with markedly altered gene expression profiles. If some samples have hidden subtypes while others do not, it may affect estimates of variation. However, I also note that the same hidden subtype factor exists for all treatment conditions and I am making inferences based on differential variation across the treatment conditions.

I hypothesized that cells in their native environment show natural single cell variability. When these cells are stressed or stimulated such as by injury signals from primary afferent neurons, a subset of the transcriptome

may respond with activation of specific pathways. I also hypothesized that such activation will have the effect of synchronizing or resetting the genes in those pathways to a coordinated expression pattern and thereby reducing variability across the samples for that subset of genes. In a temporal sequence, the transcriptome may show broad coordinated expression from the initial stress response to both injury and the collection protocol, and then subsequently relax back to their natural heterogeneous states except for the specifically activated pathways. Therefore, I reasoned that key gene classes linked to maintenance of neuropathic pain might be found amongst genes that show relatively low variation in late phase of POD7. To explore this hypothesis, I first examined the patterns of time-dependent changes in cell-to-cell heterogeneity for a collection of 172 genes hypothesized to be important in pain categorized into six functional groups relevant to microglia activation (Kettenmann et al. 2011): cytoskeleton/ECM, enzyme, GPCR, receptor, secreted molecule and transcription regulation (Table. 1). Among these, some categories such as for GPCRs and transcription regulation showed decreased cell-to-cell variation with time for the injury condition (Fig. 6C). In particular, I saw significantly lower variation in secreted molecules between POD1 and POD7 but not in the sham conditions (Fig. 6C), which might be consistent with coordinated expression of pain maintenance factors since constant release of pro-inflammatory mediators

contributes to central sensitization in spinal cord and chronic pain (Woolf 2011).

Given this observation, I carried out a screening strategy for the entire transcriptome to identify key genes by their pattern of temporal cell-to-cell variation. I examined the overlap of gene identities for the genes with time-dependent changes in their variation (Fig 5C) and classified genes into four groups according to variation change of gene expression from day 1 to day 7: Group A = estimated variation increased for both injury and sham; Group B = estimated variation increased for injury but decreased for sham; Group C = estimated variation decreased for injury but increased for sham; Group D = estimated variation decreased for both injury and sham. Amongst these groups, I expected Group C genes to be most plausible candidates for microglia activation and pain. I examined the clustering pattern of the samples using only the A, B, C, and D subset of genes by carrying out LDA projection (Fig 5D). In this figure, each dot is a 10-cell sample and the colors indicate the experimental treatments. Group C genes (56 genes; Table. 2) were particularly noticeable in inducing tight groupings of the four experimental conditions consistent with the idea that these genes were informative for distinguishing the microglia treatment states. Interestingly, Group C contains P2ry12, the gene coding P2Y12, one of the purinergic

receptor, which has been known to regulate microglia activation by increasing their expression in neuropathic pain (Haynes et al. 2006; Tozaki-Saitoh et al. 2008). These observations led us to functionally test genes selected from this group.

Validation of candidate pain genes

As mentioned above, I identified gene set of interest using two different analytic approaches: DEGs and variation analysis. Among the POD1-specific DEGs, I focused on three miRNAs (miR-137, miR-29b-1 and miR-29c) since miRNAs are known to regulate gene expression and have considerable effects on cellular functions (Sayed and Abdellatif 2011). Expression of miR-137 was increased at POD1, while expression of miR-29b-1 and miR-29c were significantly lower at POD1 (Fig. 7A). I validated miR-29c expression using real-time PCR with ipsilateral spinal cord after L4 SNT (Fig. 7B). Since P2X and P2Y signals are known to be important for pain hypersensitivity following peripheral nerve injury (Beggs et al. 2012; Kobayashi et al. 2008), I adopted in vitro ATP stimulation to activate microglia and assess the expression of these three miRNAs. Consistent with 10-cell microarray data, real-time PCR showed significant down-regulation of miR-29c (Fig. 7C) and miR-29b-1, but no up-regulation of miR-137 (data

not shown), in ATP-stimulated microglia. While miR-137 might still have expression changes, these results suggested a focus on miR-29b-1 and miR-29c as targets for in vivo functional assays. Activated microglia are known to increase the expression of pro-inflammatory cytokines such as TNFα and Il-1β, and phosphorylated p38 MAP kinase (pp38) (Ji and Suter 2007). I measured the expression of cytokines in miR-29c inhibitor-transfected microglia. MiR-29c inhibitor increased TNFα expression compared to inhibitor control group, whereas I found no difference in Il-1β mRNA expression in primary cultured microglia (Fig. 7C). I also found a significant increase of pp38 expression in the miR-29c inhibitor-transfected microglia (Fig. 7D). Together, these results were consistent with the hypothesis that miR-29c down-regulation recapitulates the cytokine responses found in activated microglia. I next examined physiological consequences of miR-29c down-regulation in microglia. Application of miR-29c inhibitor-transfected microglia elicited calcium responses in DRG neurons. (Fig. 7F). With ex vivo whole spinal cord preparation, I also found significant long-term potentiation (LTP) of evoked postsynaptic field potentials (fPSPs) in spinal dorsal horn following local application of miR-29C inhibitor-transfected microglia (Fig. 7G). Intrathecal application of activated microglia by ATP produces mechanical allodynia in rats (Tsuda et al. 2003). To dissect their role in pain, I investigated whether miR-29c inhibitor-

transfected microglia is sufficient to produce tactile allodynia when injected into naive animals. The paw withdrawal threshold decreased markedly in normal mice after intrathecal injection of miR-29c inhibitor-transfected microglia, but not in inhibitor control group (Fig. 7H), suggesting that down-regulation of microglial miR-29c in spinal cord is sufficient for developing mechanical allodynia. In addition, I tested whether miR-29c overexpressing microglia can resolve mechanical allodynia induced by ATP-stimulated microglia. Application of miR-29c mimic-transfected microglia significantly reversed mechanical allodynia, compared to control miRNA-transfected microglia at 5 hr after injection; mice injected with control miRNA was comparable to mice injected with ATP-stimulated microglia (Fig. 7I). Motor behavior, assessed by rotarod test, was not changed by microglial injection per se (data not shown). Collectively, these results suggest that down-regulation of miR-29c in microglia may play an important role in the development of neuropathic pain.

Next, I focused on 56 genes found through temporal variation analysis (Group C; see above) to assess whether any of these genes may play a role in the development/maintenance of neuropathic pain. Based on information from previous literature, I have selected nine genes (Hexb, Gria1, Glul, P2ry12, Trf, Spg21, Cdk5, Bank1, Arf6) out of 56 genes. The

rest of 47 genes have been excluded for the further experiments since they have neither been studied in Pain field nor in other research fields. I tested changes in the expression level of the nine genes in the ipsilateral spinal cord at POD7. Of the nine genes, only P2ry12 expression showed significant difference between sham and POD7, but I found no significant difference in other eight genes (Fig. 8A). Because microglial changes could be masked in the whole spinal cord tissue, I additionally tested expression changes under in vitro ATP stimulation conditions. Under ATP simulation, I only found a significant change in the expression of Gria1, the gene encoding AMPA receptor subunit GluA1, both at mRNA and protein levels (Fig. 9A, B), but not for the other eight genes (Fig. 9B). Immunofluorescence analysis revealed that microglia stained with Iba-1 expressed GluA1 in resting state, while its expression significantly decreased when microglia were treated with ATP (Fig. 9B). A previous study suggested that activation of AMPA receptor by glutamate promotes release of TNFα whereas the potentiation of microglial AMPA receptors by AMPA receptors agonist inhibits TNFα release (Hagino et al. 2004). Microglial Gria1 knockdown induced TNFα release as well as increased mRNA expression (Fig. 9C, D). I tested live animal response to Gria1 expression changes by intrathecal injection of siGria1 microglia. Similar to the results for miR-29c, I found that microglial Gria1 knockdown produced mechanical

allodynia. Paw withdrawal threshold decreased only after the injection of siGria1 microglia, but not of siScram microglia (Fig. 9E). With administration of etanercept (1 mg, i.p.), a TNFα inhibitor, 1 hr after injection of siGria1 microglia, siGria1 microglia-induced pain was significantly reversed at 5 hr after microglial injection (Fig. 9F). Taken together, these results suggest that Gria1 down-regulation may contribute to mechanical allodynia via TNFα production.

Fig. 1. Experimental design for microarray with 10 pooled spinal microglia after L4 SNT

(A) Left, L4 SNT microglia were compared to sham microglia after nerve injury at day1 and day7, respectively. Right, Mechanical threshold was measured in sham and L4 SNT mice 1, 3 and 7 days after surgery (n=12 for each experimental group, total n=24 mice). Mechanical allodynia was fully developed at POD7. p=0.0432 for day1; p=0.006 for day3; p=0.0070 for day7 compared to respective sham controls. Data are shown as means ± SEM. (B) Representative images of GFP-labeled microglia (green) in spinal cord of mouse at POD1 and POD7 after L4 SNT. Scale bar: 100 μm (C) Images showing individual collection of spinal microglia into a glass pipette. Scale bar: 40 μm. (D) A representative image of 10 pooled-cell RT PCR analysis showing the expression of CD11b, a well-known microglia marker, in 10 pooled microglia (MG) and the PC but not in NC. β-actin was used as a endogenous positive control. cDNA from primary cultured microglia was used as a PC. M, a marker for DNA size; PC, positive control; NC, negative control.

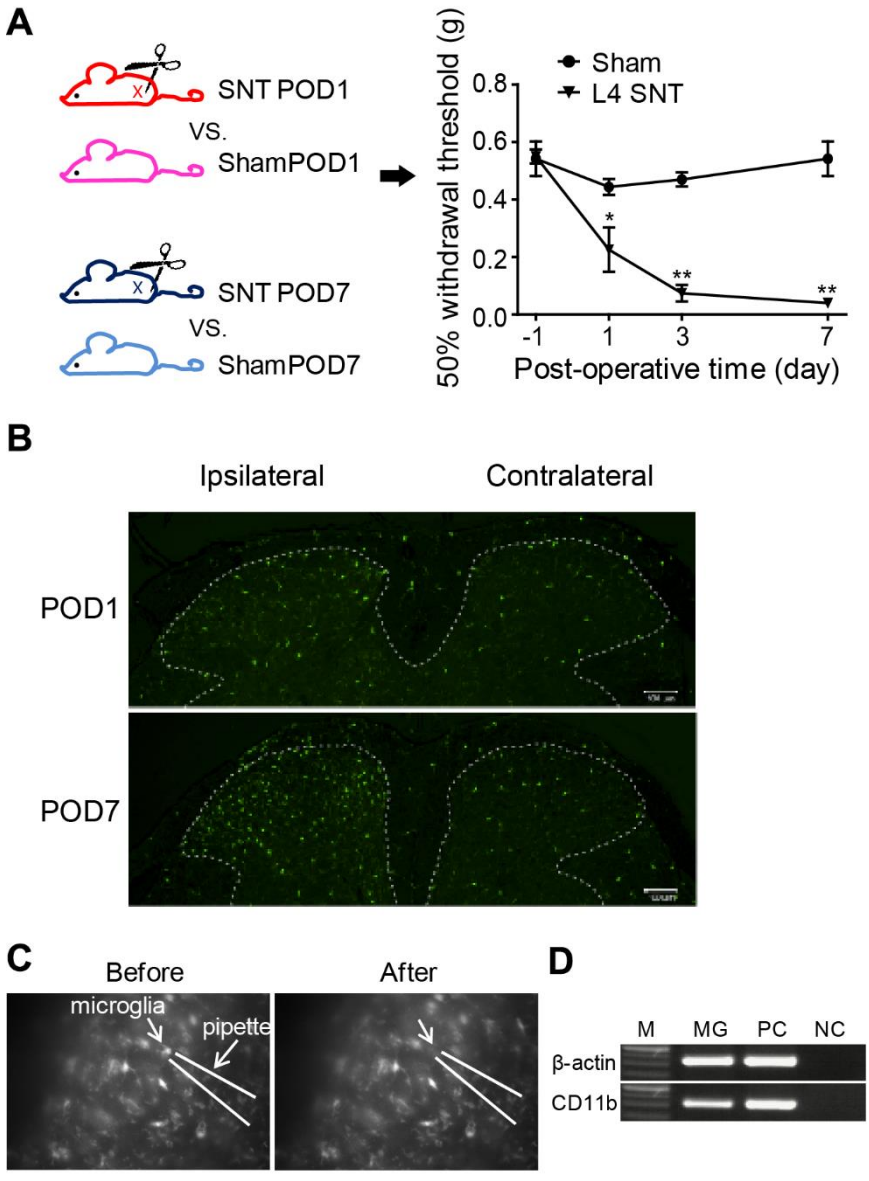
A
SNT POD1
VS.
ShamPOD1
SNT POD7
VS.
ShamPOD7
50% withdrawal threshold (g)
0.8
0.6
0.4
0.2
0.0
Sham
L4 SNT
*
**
**
-1
1
3
7
Post-operative time (day)
B
Ipsilateral
Contralateral
POD1
POD7
C
Before
After
microglia
pipette
D
M
MG
PC
NC
β-actin
CD11b

Fig. 2. Validation of single-cell microarray data

(A) A heat map of expression profile with 14 known microglia genes associated with neuropathic pain, comparing injury group to sham-operated group at POD1 and POD7, respectively. No significant changes were detected in expression level of housekeeping genes between sham- and SNT-microglia. Marker genes for other CNS cell types were used as negative control. (B) A heat map of expression profile of 28 spinal microglia-specific genes. (C) A heat map of expression profile of 40 brain-derived-microglial unique genes. (D) Validation of single-cell microarray data using single-cell microarray samples by real-time PCR, which revealed up-regulation of Il-1β, Tnfα, C5aR1, Cx3cr1, P2rx4. Data are shown as means ± SEM. (E) A summarizing graph showing that expression changes of the different sets of genes. Previously known microglial genes were up-regulated. Other CNS cell types and housekeeping genes were used as negative control.

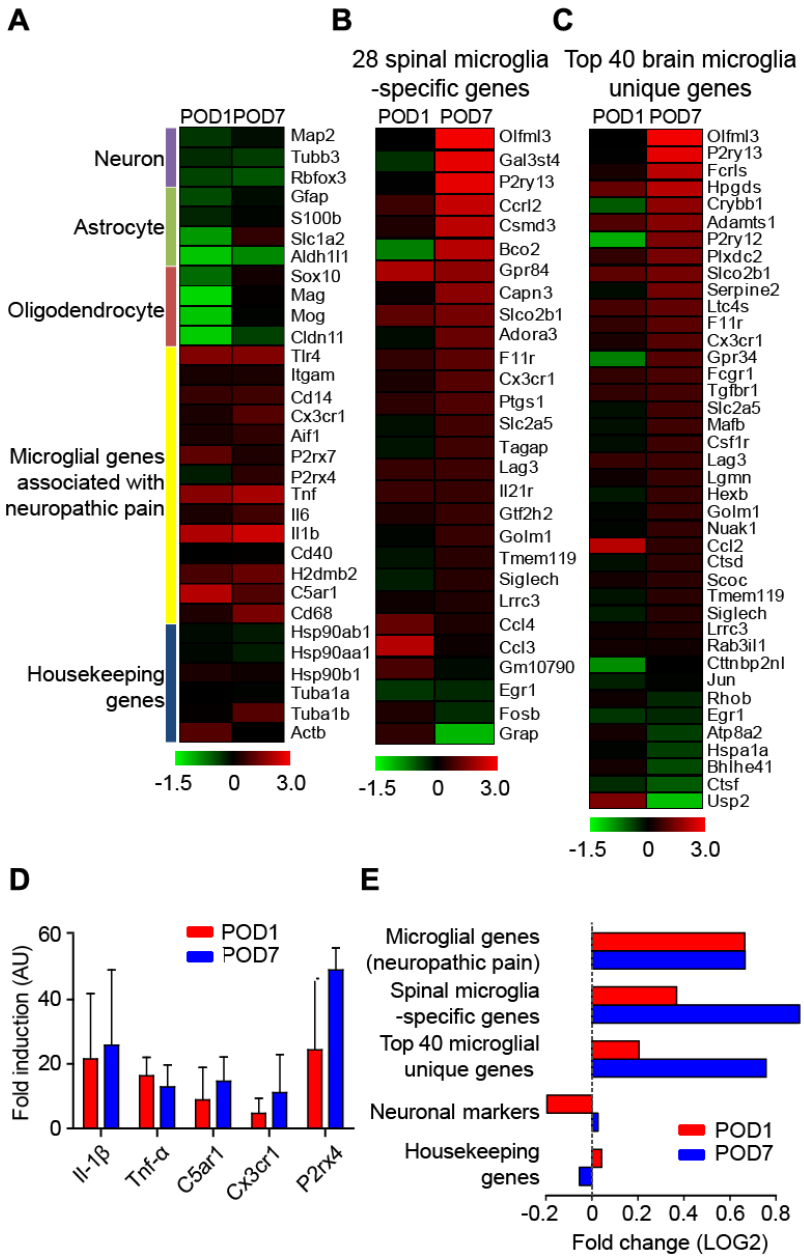
A
B
C
28 spinal microglia -specific genes
Top 40 brain microglia unique genes
POD1 POD7
Neuron
Astrocyte
Oligodendrocyte
Microglial genes associated with neuropathic pain
Housekeeping genes
Map2
Tubb3
Rbfox3
Gfap
S100b
Slc1a2
Aldh1l1
Sox10
Mag
Mog
Cldn11
Tlr4
Itgam
Cd14
Cx3cr1
Aif1
P2rx7
P2rx4
Tnf
Il6
Il1b
Cd40
H2dmb2
C5ar1
Cd68
Hsp90ab1
Hsp90aa1
Hsp90b1
Tuba1a
Tuba1b
Actb
-1.5 0 3.0
Olfml3
Gal3st4
P2ry13
Ccrl2
Csmd3
Bco2
Gpr84
Capn3
Slco2b1
Adora3
F11r
Cx3cr1
Ptgs1
Slc2a5
Tagap
Lag3
Il21r
Gtf2h2
Golm1
Tmem119
Siglech
Lrrc3
Ccl4
Ccl3
Gm10790
Egr1
Fosb
Grap
Olfml3
P2ry13
Fcrls
Hpgds
Crybb1
Adamts1
P2ry12
Plxdc2
Slco2b1
Serpine2
Ltc4s
F11r
Cx3cr1
Gpr34
Fcgr1
Tgfbr1
Slc2a5
Mafb
Csf1r
Lag3
Lgmn
Hexb
Golm1
Nuak1
Ccl2
Ctsd
Scoc
Tmem119
Siglech
Lrrc3
Rab3il1
Cttnbp2nl
Jun
Rhob
Egr1
Atp8a2
Hspa1a
Bhlhe41
Ctsf
Usp2
D
E
Fold induction (AU)
60
40
20
0
POD1
POD7
Il-1β
Tnf-α
C5ar1
Cx3cr1
P2rx4
Microglial genes (neuropathic pain)
Spinal microglia -specific genes
Top 40 microglial unique genes
Neuronal markers
Housekeeping genes
POD1
POD7
-0.2 0 0.2 0.4 0.6 0.8
Fold change (LOG2)

Fig. 3. Expression of unique microglial genes in single-cell microarray data

(A) Expression profile of 28 spinal microglia-specific genes in each array sample in the pseudo-color scheme. (B) Expression profile of 40 brain-derived-microglial unique genes in the pseudo-color scheme.

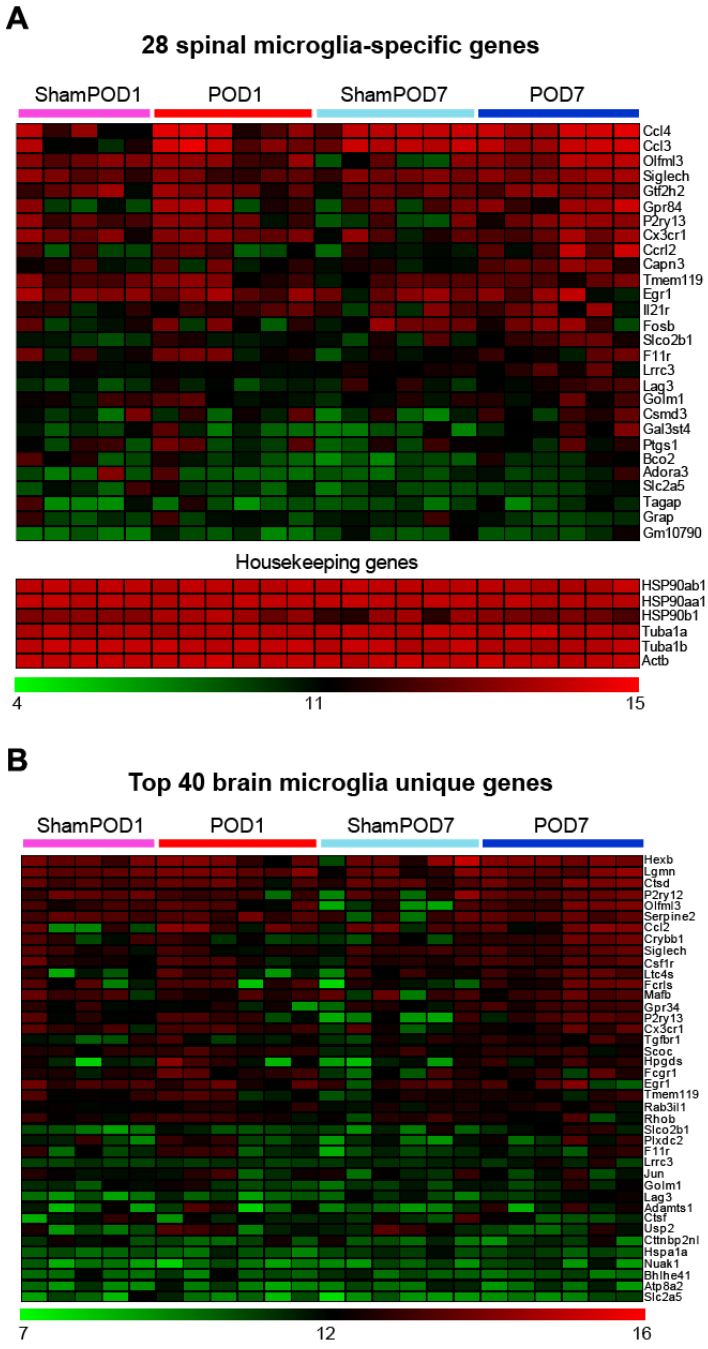
A
28 spinal microglia-specific genes
ShamPOD1
POD1
ShamPOD7
POD7
Ccl4
Ccl3
Olfml3
Siglech
Gtf2h2
Gpr84
P2ry13
Cx3cr1
Ccrl2
Capn3
Tmem119
Egr1
Il21r
Fosb
Slco2b1
F11r
Lrrc3
Lag3
Golm1
Csmd3
Gal3st4
Ptgs1
Bco2
Adora3
Slc2a5
Tagap
Grap
Gm10790
Housekeeping genes
HSP90ab1
HSP90aa1
HSP90b1
Tuba1a
Tuba1b
Actb
4
11
15
B
Top 40 brain microglia unique genes
ShamPOD1
POD1
ShamPOD7
POD7
Hexb
Lgmn
Ctsd
P2ry12
Olfml3
Serpine2
Ccl2
Crybb1
Siglech
Csf1r
Ltc4s
Fcrls
Mafb
Gpr34
P2ry13
Cx3cr1
Tgfbr1
Scoc
Hpgds
Fcgr1
Egr1
Tmem119
Rab3il1
Rhob
Slco2b1
Plxdc2
F11r
Lrrc3
Jun
Golm1
Lag3
Adamts1
Ctsf
Usp2
Cttnbp2nl
Hspa1a
Nuak1
Bhlhe41
Atp8a2
Slc2a5
7
12
16

Fig. 4. Time-dependent differential expression changes of spinal microglial genes after peripheral nerve injury

(A) Venn diagram showing the number of up- and down-regulated genes meeting fold change (Log2) > 1.5 and statistical thresholds ($p > 0.05$ by t-test) in each time point. (B) Gene expression profile of DEGs grouped into three clusters (POD1-specific, POD7-specific and common genes) in the pseudo-color scheme. (C-D) Strong regulated microglial genes according to biological process (C) and cellular component (D) in each time point. Red, POD1; Blue, POD7; Yellow, common DEGs.

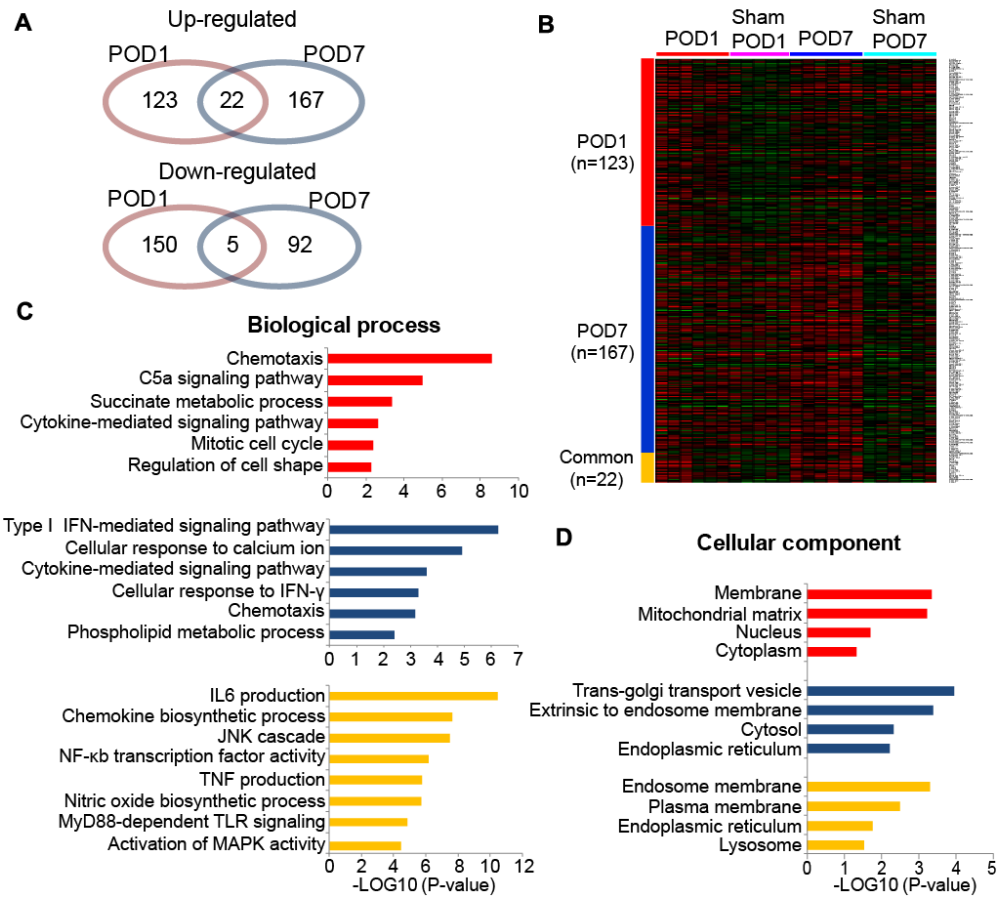
A
Up-regulated
POD1
POD7
123
22
167
Down-regulated
POD1
POD7
150
5
92
B
POD1
Sham POD1
POD7
Sham POD7
POD1 (n=123)
POD7 (n=167)
Common (n=22)
C
Biological process
Chemotaxis
C5a signaling pathway
Succinate metabolic process
Cytokine-mediated signaling pathway
Mitotic cell cycle
Regulation of cell shape
0 2 4 6 8 10
Type I IFN-mediated signaling pathway
Cellular response to calcium ion
Cytokine-mediated signaling pathway
Cellular response to IFN-γ
Chemotaxis
Phospholipid metabolic process
0 1 2 3 4 5 6 7
IL6 production
Chemokine biosynthetic process
JNK cascade
NF-κb transcription factor activity
TNF production
Nitric oxide biosynthetic process
MyD88-dependent TLR signaling
Activation of MAPK activity
0 2 4 6 8 10 12
-LOG10 (P-value)
D
Cellular component
Membrane
Mitochondrial matrix
Nucleus
Cytoplasm
Trans-golgi transport vesicle
Extrinsic to endosome membrane
Cytosol
Endoplasmic reticulum
Endosome membrane
Plasma membrane
Endoplasmic reticulum
Lysosome
0 1 2 3 4 5
-LOG10 (P-value)

Fig. 5. Identification of candidate pain-maintenance neuropathic microglial genes by variation analysis

(A) MDS plots of the spinal microglia transcriptome. Left panel shows the dispersion using only six housekeeping genes (Tuba1a, Tuba1b, Hsp90ab1, Hsp90aa1, Hsp90b1, and Actb) as negative control. Right panel shows the dispersion using all genes (20,694 genes including the housekeeping genes). Each dot represents pooled ten microglia. (B) Box plot of the JSD of the transcriptome amongst samples of the same cell type, which captures the information-theoretic difference between two distributions (i.e., transcriptomes). (C) A venn diagram showing the overlap of gene identities of entire transcriptome with time-dependent changes in their variation. (D) LDA plots showing classified genes into four groups according to variation change from day 1 to day 7 after nerve injury. In particular, the group C genes (56 genes) show clearly distinct clustering patterns within the groups. Group A, variation increased for both injury and sham; Group B, variation increased for injury but decreased for sham; Group C, variation decreased for injury but increased for sham; Group D, variation decreased for both injury and sham.

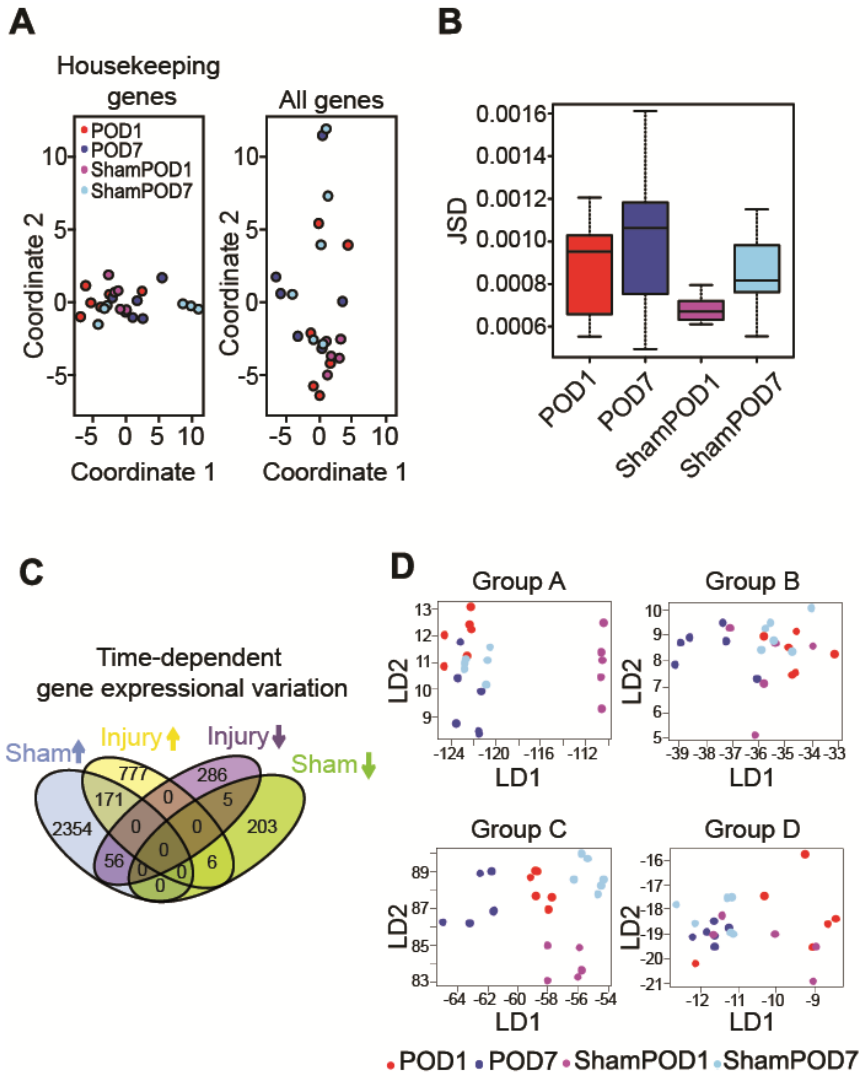
A
Housekeeping genes
All genes
POD1
POD7
ShamPOD1
ShamPOD7
Coordinate 1
Coordinate 2
B
JSD
POD1
POD7
ShamPOD1
ShamPOD7
C
Time-dependent gene expressional variation
Sham
Injury
Injury
Sham
777
286
171
0
5
2354
0
0
203
0
56
0
0
6
0
D
Group A
Group B
Group C
Group D
LD1
LD2
POD1 POD7 ShamPOD1 ShamPOD7

Fig. 6. Time-dependent variation changes of gene expression in spinal microglia after peripheral nerve injury.

(A) Distribution of coefficient of variation (CV) values showing within-group variability. Whole genes (23453 genes) were tested for each group. Data are expressed as SD/mean. (B) The number of genes showing variation changes over time tested by an F-test for ratio of variance (POD7/POD1 and Sham POD7/Sham POD1) of each gene. Whole genes (23453 genes) were tested both in sham and injury groups. (C) CVs showing pattern of changes in expressional variation of six selected gene categories for microglia activation after nerve injury; cytoskeleton/extracellular matrix (ECM), enzyme, GPCR, receptor, secreted molecule and transcription regulation (See Table. 2 for the gene lists). Housekeeping genes and whole genes were used as control. Data are expressed as SD/mean.

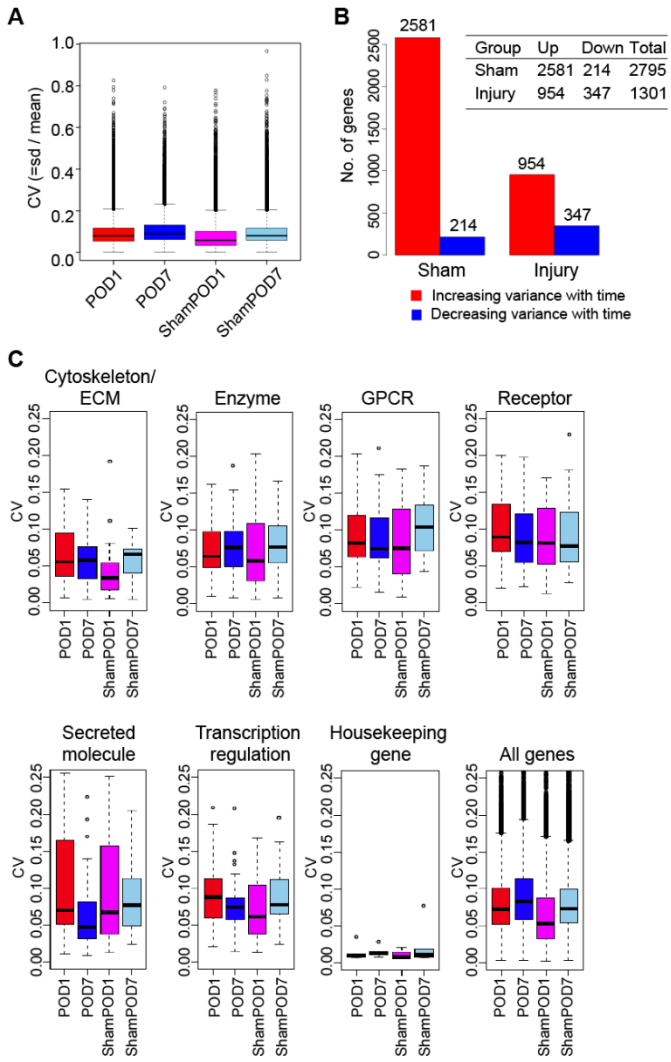
A
CV (=sd / mean)
POD1
POD7
ShamPOD1
ShamPOD7
B
No. of genes
2581
214
954
347
Sham
Injury
Increasing variance with time
Decreasing variance with time
Group Up Down Total
Sham 2581 214 2795
Injury 954 347 1301
C
Cytoskeleton/ ECM
Enzyme
GPCR
Receptor
Secreted molecule
Transcription regulation
Housekeeping gene
All genes
CV

Fig. 7. Spinal administration of miR-29c knockdown microglia in normal mice produces mechanical allodynia via microglia activation

(A) Fold changes of microRNAs, miR-137, miR-29b-1 and miR-29c, which were significantly changed exclusively at POD1 in spinal microglia after nerve injury. (B) Relative expression of miR-29c in ipsilateral spinal cord 1 day after L4 SNT. (C) Validation of miR-29c expression using primary cultured microglia activated by ATP application (50 μM, for 1 hr) by real-time qPCR. Data are normalized against RNU6B. (D) Changes in mRNA expression of cytokines, TNFα and Il-1β, in miR-29c inhibitor-transfected microglia using real-time qPCR. (E) Expression of pp38 revealed by western blot analysis in each group. The relative amount of pp38 protein was normalized to expression level of p38 in inhibitor control and miR-29c inhibitor-transfected microglia. (F) Increased intracellular calcium in primary DRG neurons by miR-29c inhibitor-transfected microglia. Top, the average (means ± SEM) traces of $[Ca^{2+}]_i$ changes in all DRG neurons with microglia treatment from one particular imaging experiment. Bottom, summary of Ca^{2+} transient responses in DRG neurons to the microglia application in an unbiased manner. $P < 0.0001$. (G) LTP of fPSPs induced by miR-29c inhibitor-transfected microglia application. Insets show representative traces from one experiment at baseline (1) and 120 min (2). Two-way repeated measures ANOVA. $P = 0.0015$. (H) Paw withdrawal

threshold after intrathecal injection of miR-29c inhibitor-transfected microglia into naïve mice. Microglia transfected with inhibitor control was used as control. n=6 for inhibitor control, n=7 for miR-29c inhibitor. *p < 0.05 , ***p < 0.001. (I) Paw withdrawal threshold after intrathecal injection of miR-29c mimic-transfected microglia following ATP stimulation. ATP-treated microglia was used as positive control. n=6 for ATP-treated microglia, n=6 for control miRNA and ATP microglia, n=8 for miR-29c mimic and ATP mciroglia. *p < 0.05 compared to control miRNA and ATP microglia at 5hr. See Fig. 10C, D for efficacy of miR-29c inhibitor, miRNA mimic. All data in this figure are shown as means ± SEM unless otherwise stated.

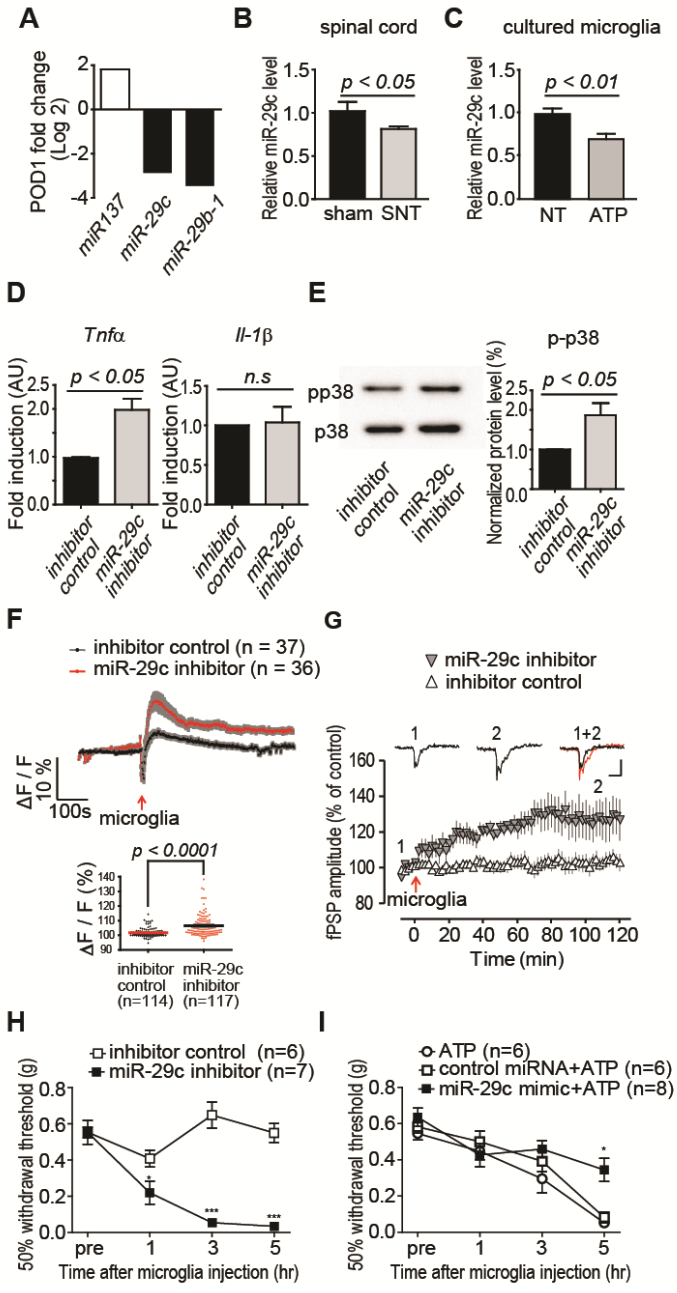
A
POD1 fold change (Log 2)
miR137
miR-29c
miR-29b-1
B
spinal cord
Relative miR-29c level
p < 0.05
sham
SNT
C
cultured microglia
Relative miR-29c level
p < 0.01
NT
ATP
D
Tnfα
Il-1β
Fold induction (AU)
p < 0.05
n.s
inhibitor control
miR-29c inhibitor
E
pp38
p38
p-p38
Normalized protein level (%)
p < 0.05
F
inhibitor control (n = 37)
miR-29c inhibitor (n = 36)
ΔF / F 10 %
100s
microglia
p < 0.0001
ΔF / F (%)
inhibitor control (n=114)
miR-29c inhibitor (n=117)
G
miR-29c inhibitor
inhibitor control
fPSP amplitude (% of control)
microglia
Time (min)
H
inhibitor control (n=6)
miR-29c inhibitor (n=7)
50% withdrawal threshold (g)
Time after microglia injection (hr)
I
ATP (n=6)
control miRNA+ATP (n=6)
miR-29c mimic+ATP (n=8)
50% withdrawal threshold (g)
Time after microglia injection (hr)

Fig. 8. Validation of candidate pain genes.

(A) Real-time qPCR analysis showing expressional changes of nine candidate target genes (P2ry12, Cdk5, Glul, Spg21, Trf, Hexb, Arf6, Bank1, Gria1) among group C genes in ipsilateral spinal cord at POD7. Significance compared to sham control. Data are normalized against Gapdh. Data are represented as mean ± SEM. (B) Real-time qPCR analysis showing expressional changes of eight candidate target genes (P2ry12, Cdk5, Glul, Spg21, Trf, Hexb, Arf6, Bank1) among group C genes under ATP-stimulated microglia activation condition, which revealed no significant changes in expression level compared to vehicle control. Data are normalized against Gapdh. Data are represented as mean ± SEM. (C) Real-time qPCR showing efficacy of siGria1. Data are represented as mean ± SEM. (D) Real-time qPCR analysis showing Gria1 mRNA level in miR-29c inhibitor-transfected microglia compared to inhibitor control. Data are represented as mean ± SEM. n.s, not significant.

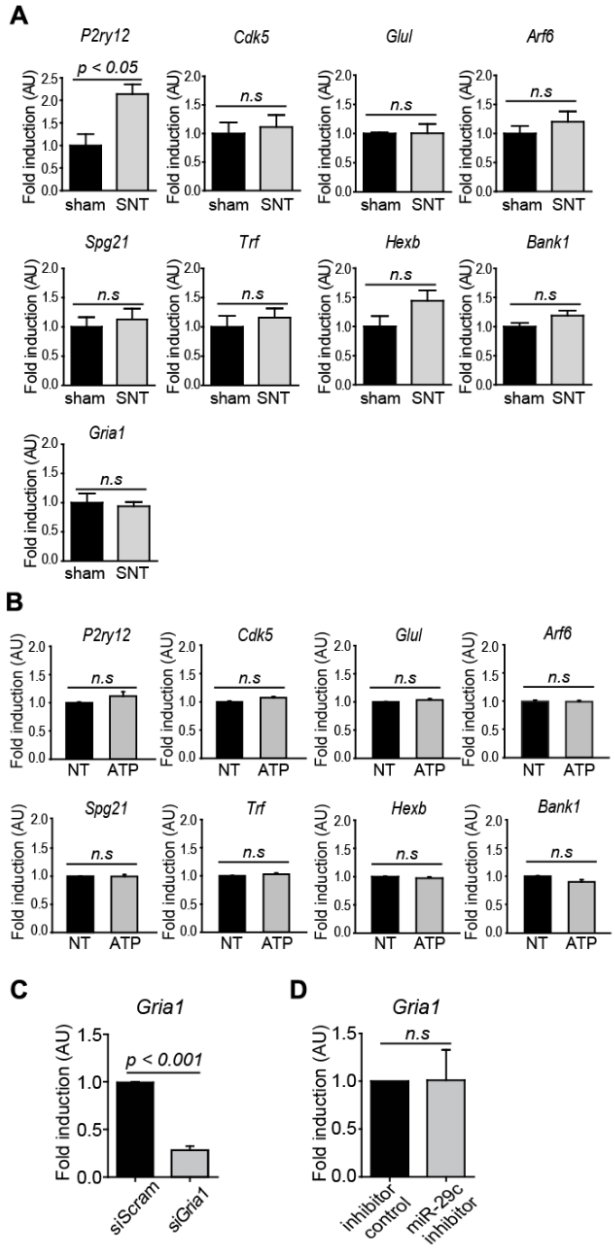
A
P2ry12
p < 0.05
Cdk5
n.s
Glul
n.s
Arf6
n.s
Spg21
n.s
Trf
n.s
Hexb
n.s
Bank1
n.s
Gria1
n.s
Fold induction (AU)
sham
SNT
B
P2ry12
n.s
Cdk5
n.s
Glul
n.s
Arf6
n.s
Spg21
n.s
Trf
n.s
Hexb
n.s
Bank1
n.s
NT
ATP
C
Gria1
p < 0.001
siScram
siGria1
D
Gria1
n.s
inhibitor control
miR-29c inhibitor

Fig. 9. Spinal administration of Gria1 knockdown-microglia in normal mice produces mechanical allodynia reversed by TNFα inhibitor

(A) Validation of Gria1 expression using primary cultured microglia activated by ATP application (50 μM, for 1 hr) by real-time qPCR. (B) Immunofluorescence of GluR1 (red) in primary cultured microglia following ATP (50 μM, for 1 hr) application. Scale bar: 20 μm. (C) Increased TNFα mRNA in siGria1 microglia compared to siScram revealed by real-time qPCR. (D) Increased TNFα release in siGria1 microglia measured by ELISA. (E) Paw withdrawal threshold after intrathecal injection of siGria1 microglia into naïve mice. siScram was used as negative control. n=6 for siScram, n=7 for siGria1. *** $p < 0.001$. (F) Etanercept reversed the paw withdrawal threshold which was produced by intrathecal injection of siGria1 microglia. N=7 for siGria1, n=6 for siScram and etanercept, n=10 for siGria1 and etanercept. **$p < 0.01$ compared to siGria1 group. siGria1, siGria1 transfected microglia; siScram, Scrambled siRNA transfected microglia. See Fig. 8C for efficacy of Gria1 siRNA. All data in this figure are shown as means ± SEM.

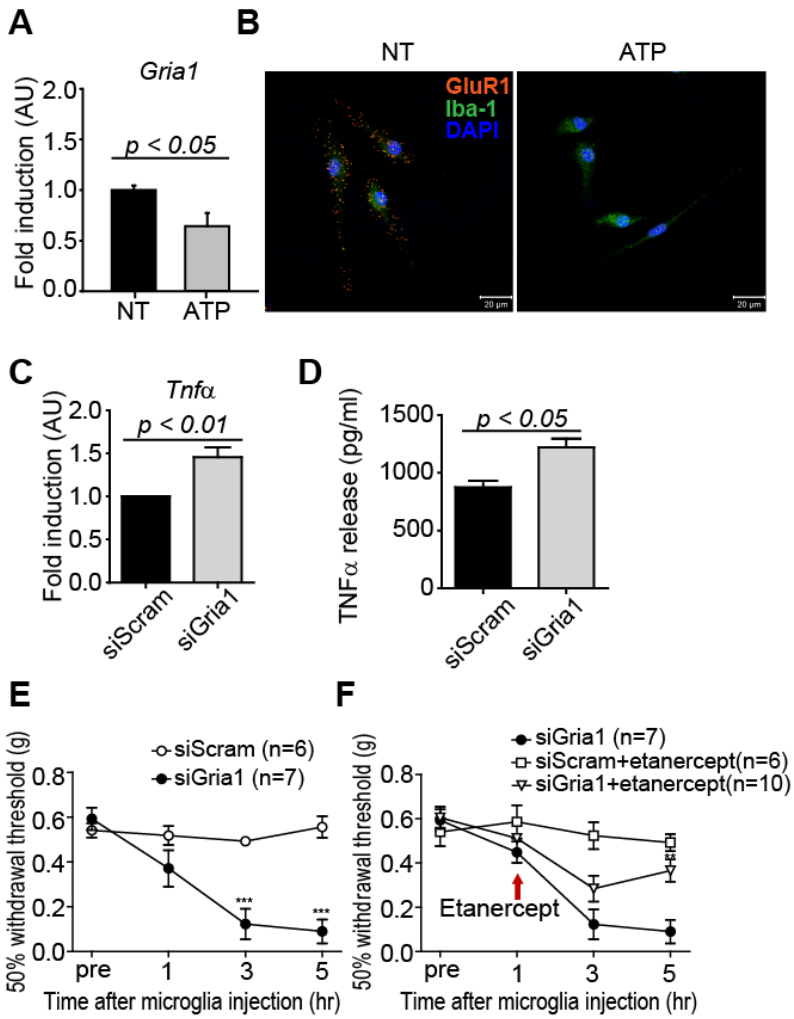
A
Gria1
p < 0.05
Fold induction (AU)
2.0
1.5
1.0
0.5
0.0
NT
ATP
B
NT
ATP
GluR1
Iba-1
DAPI
20 μm
C
Tnfα
p < 0.01
Fold induction (AU)
siScram
siGria1
D
p < 0.05
TNFα release (pg/ml)
1500
1000
500
0
siScram
siGria1
E
siScram (n=6)
siGria1 (n=7)
50% withdrawal threshold (g)
0.8
0.6
0.4
0.2
0.0
***
***
pre
1
3
5
Time after microglia injection (hr)
F
siGria1 (n=7)
siScram+etanercept(n=6)
siGria1+etanercept(n=10)
50% withdrawal threshold (g)
Etanercept
pre
1
3
5
Time after microglia injection (hr)

Fig. 10. In situ hybridization expression of miR-29c in spinal dorsal horn after nerve injury.

(A) Decreased expression of miR-29c in spinal dorsal horn at POD1 compared to sham control. (B) Identification of miR-29c expression in spinal cord. Astrocytes (top), microglia (middle) and neuron (bottom) labeled with antibodies to GFAP, IBA1, and NeuN, respectively. Scale bar: 50 μm. (C) Real-time qPCR showing efficacy of miR-29c inhibitor. Data are represented as mean ± SEM. (D) Real-time qPCR showing efficacy of miR-29c mimic Data are normalized against RNU6B. Data are represented as mean ± SEM.

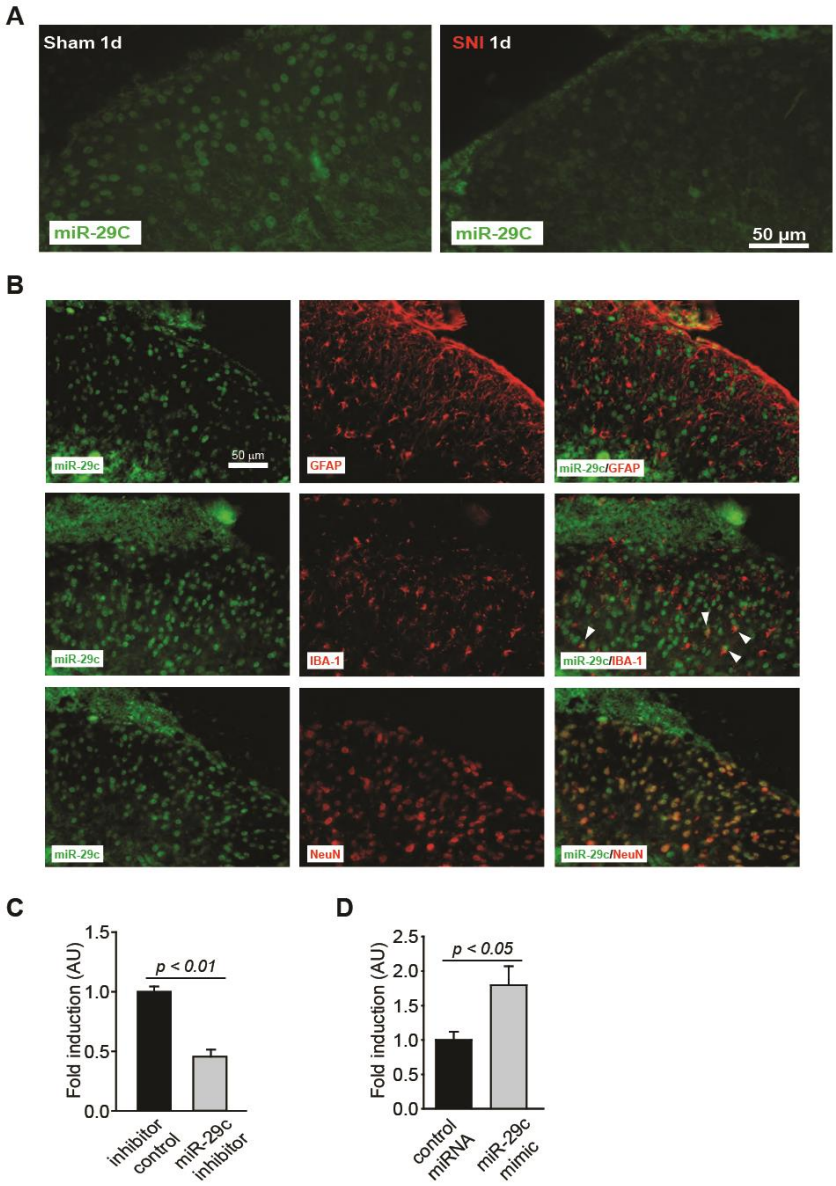
A
Sham 1d
miR-29C
SNI 1d
miR-29C
50 µm
B
miR-29c
50 µm
GFAP
miR-29c/GFAP
miR-29c
IBA-1
miR-29c/IBA-1
miR-29c
NeuN
miR-29c/NeuN
C
Fold induction (AU)
1.5
1.0
0.5
0.0
p < 0.01
inhibitor control
miR-29c inhibitor
D
Fold induction (AU)
2.5
2.0
1.5
1.0
0.5
0.0
p < 0.05
control miRNA
miR-29c mimic

Table.1 Gene list of six category genes

GPCR	Secreted molecules (cytokine, chemokine, fractalkine)	Cytoskeleton/ ECM	Receptor	Transcription regulation	Enzyme
Lpar1	Ccl2	Dpysl3	Tlr2	Irf8	Srpk3
Lpar3	Ccl5	Appbp2	Tlr4	Runx1t1	Dusp1
C3ar1	Ccl6	Cfl1	Tlr7	Cbfa2t3	Dusp16
C5ar1	Cxcl10	Marcks	P2rx4	Sfxn1	Gch1
P2ry6	Nos2	Mmp9	P2rx7	Sgpl1	Pld2
Ccr5	Il2rg	Mmp2	Csf1r	Six1	Ppip5k2
Gpr56	Pros1	Lgals3	F11r	Stat5a	Pten
P2ry12	C1qa	Aif1	Cd34	Xrcc4	Mmp9
P2ry13	C1qb	Cav1	Cd53	Nkap	Mmp2
Cx3cr1	C1qc	Map1b	Cd68	Nfkb1	MAPK8
Ptger2	Il1b	Coro1a	Hvcn1	Nfkb2	MapK1
Ptger4	Il6	Arpc1b	Clic1	Atf3	MapK3
Cnr2	Tnf	Timp2	Kcnn4	Stat3	MapK7
Bdkrb1	Bdnf	Tpm3	Kcnn1	Trp53	MapK11
Bdkrb2	Ctss	Nefh	Kcnn2	Creb1	MapK12
Tacr1	Il18	Mmp7	Kcnn3	Creb3	MapK13
Grm1	Il1a	Ncam1	Kcnj2	Creb5	MapK14
Grm2	Il10	Ncam2	Cd200r1	Crebbp	Casp3
Grm3	Ccl3	Icam1	Cd40	Crtc1	Casp7
Grm4	Ccl4	Hmgb1	Ifngr1	Crtc2	Casp8
Grm5	Ctsb		Trpv1	Crtc3	Camk2a
Gpr84	Ctsh		Trpv4	Spi1	Camk2b
Htr2b	Grn		Trpm2	Nfatc1	NOS2
Gpr132	Tgfb1		H2-dmb2	Nfatc2	Capn1
			Cd37	Stat1	Ctsb
			H2-dma	Rela	Ptk2
			Fcgr2b	Fos	Hexb
			Csf3r	Jun	Ptges

			Panx1	Rel Smad3	Ptges2 PTPRC Lpcat1 Hmox1 Mmp13 Ptgs1 Ptgs2 Sod1 Jak1 Jak2 Jak3 Parp1 Pla2g2a Pla2g4a Map2k1 Cdk5

Table. 2 Gene list of four groups based on microglial cell-to-cell variation analysis

Group A (n=171)	Group B (n=6)	Group C (n=56)	Group D (n=5)
1700066M21Rik	Krt24	Glul	Zdhhc17
Agxt	Adarb2	Mrps14	Lrrn4cl
Capza1	Cideb	Gng7	CK137956
Serpinb2	9830147E19Rik	Bloc1s1	Zfp568
Mki67ip	Tmem170	Gria1	Itgb1
Uchl5	Rdx	Tex14	
Sele		0610010K14Rik	
Cnih4		Psma6	
Kif1a		Dnajb6	
Tsn		Arf6	
Zbtb37		Kif4-ps	
B020018G12Rik		Rian	
Adss		AF357355	
Spata17		Gm10767	
Gm10825		Mier3	
Ppa1		Hexb	
Krtap12-1		Duxbl1	
Olfr1355		Galnt15	
Mfsd12		Psmb5	
Olfr774		Cyc1	
Pcmt1		Nudt16l1	
Amd1		7120432I05Rik	
Ddt		Hagh	
Plekhj1		Pcdhb13	
Mrpl54		Mrpl43	
Myrfl		Cir1	
Cct2		Olfr988	

9530003J23Rik		Ciao1		
Asb3		Zc2hc1a		
Spop		Krtcap2		
Mrpl45		Mir137		
Tubg2		Impa1		
Gabrg2		P2ry12		
1700024J04Rik		Fdps		
Olfr329-ps		Prok1		
6330403K07Rik		Bank1		
Eif2s1		Bspry		
Vsx2		Laptm5		
Fcf1		BC049635		
Vti1b		Trappc2		
Asb2		Wipi2		
Vmn1r218		Cdk5		
Rala		1500011B03Rik		
BC061237		Psmg3		
Npy4r		Tprkb		
AU040096		Sox5		
Tas2r119		BC089491		
Polr2f		Use1		
Aco2		Fgl1		
Cldn16		Spg21		
Hspbap1		Cdkn2d		
Prm2		Map2k1		
Fopnl		Trf		
Iglv1		BC147527		
Iqcg		Olfr1324		
Mrgprh		Tsc22d3		
Cyp4f40				
Slc44a4				
7330403C04Rik				
Olfr120				

Mea1				
Treml4				
4930505H01Rik				
Cript				
Prss22				
Nkx2-5				
Hsf2bp				
2610034M16Rik				
1700011E24Rik				
Chmp3				
Gpr17				
Pfdn1				
Mir378				
Nars				
Rcor2				
Gstp1				
Scgb1a1				
1700025F22Rik				
Eif3a				
Phyh				
Rapgef1				
Fam129b				
Gm13498				
Ssb				
Ckmt1				
Ctxn2				
AU019990				
Gm561				
Cdc123				
Itih2				
Nacc2				
Pla2r1				
Olfr1044				

Olfr1053				
Prdm11				
Accs				
Ell3				
Prokr2				
Sec62				
Dpm3				
Pmvk				
Pear1				
Gm10696				
Cdh17				
Ldlrad1				
Ptch2				
Tnfrsf25				
Aqp7				
Mup4				
Stmn1				
2310002L09Rik				
Fam154a				
Gm12597				
Utp11l				
Gm15772				
4930511M11Rik				
2900005J15Rik				
Otop1				
Cxcl15				
Anxa3				
Oasl1				
Bud31				
G3bp2				
Cxcl11				
Hscb				
Vmn1r13				

M6pr				
Dppa3				
Tas2r113				
Klf14				
Vmn1r23				
Eogt				
Vmn1r79				
Cabp5				
Sycn				
Klk9				
Gm9999				
Vmn2r77				
Olfr574				
Olfr631				
Olfr481				
1110004F10Rik				
Scgb2b20				
Snord35b				
Mrgpra6				
4933402N03Rik				
Star				
Mrpl34				
Impdh2				
4933405L10Rik				
Gm10280				
Cmtm2a				
Lctl				
Fam96a				
Nckipsd				
Olfr937				
Olfr984				
Paqr5				
Nradd				

Ccr4			
Slc22a13			
Mir676			
Wbp5			
Gpr143			
Asb11			
Pqbp1			
Dynlt3			
Cetn2			
4930595M18Rik			
Gm20767			
Noc2l			

DISCUSSION

In this study, I adopted a high resolution, individually collected, transcriptome assay to screen for microglia-specific factors for the first time in a rodent neuropathic pain model. Mechanical collection of marked microglia allowed assessment of pure cell populations for expression changes resulting in an unbiased (up to probes on the microarray) discovery process. Furthermore, this approach allowed further examination of the diversity of gene profiles within multiple small pools of cells coupled with a time-dependent variation analysis resulting in a novel approach for candidate gene discovery. Many microglial changes could be masked in the analysis with the whole spinal cord tissue (Fig. 8A), and analyses based on cell variation would not have been possible with whole tissue level data. Heterozygous $Cx3cr1^{+/GFP}$ male mice were used to visualize spinal microglia in this study. Although recent studies have been reported that Cx3cr1 deficiency affects microglia activation status, and could ameliorate or worsen pathology (Cardona et al. 2006; Lee et al. 2010), I could find evidently increased GFP-positive cells in ipsilateral spinal cord of $Cx3cr1^{+/GFP}$ mouse after nerve injury.

From the experiments presented in this thesis, I found down-

regulated miR-29c in early spinal microglia as a possible factor for the microglia activation and the initiation/development of neuropathic pain as well as the possible role of Gria1, the gene encoding AMPA receptor subunit GluA1, in time-dependent injury and pain response. GO analysis further suggested that early and late microglia could have functionally distinct phenotypes following peripheral nerve injury even though they are difficult to distinguish by morphology alone.

1. Validity of transcriptome analysis

Despite being obtained from a very small number of cells, gene profile of previously known genes from this transcriptome data was largely consistent with general expectations from previous studies. Our 10-cell microglia data contained many spinal microglia-specific genes recently reported by Chiu et al (Fig. 2B) (Chiu et al. 2013). I also minimized the possibility of contamination of infiltrating macrophage, given that brain microglia signature genes but not the peripheral monocyte signature genes were enriched in this microarray data (Butovsky et al. 2014). Indeed, recent studies have suggested that infiltrating macrophages may not contribute to the neuropathic pain after peripheral nerve injury (Grace et al. 2014).

2. Distinctive transcriptome profiles of early and late phase

microglia

I found early microglia genes that are actively responding to peripheral nerve injury, leading to up-regulation of receptors and channels at POD1 (and in some case at POD7 as well). Notably, in addition to the toll-like receptor (TLR) 4 previously shown to be up-regulated after nerve injury (Bettoni et al. 2008), I also identified other toll-like receptors such as TLR7 and TLR13, which could be also important for the microglia activation and neuropathic pain. Interestingly, a recent study showed that extracellular miRNAs can activate nociceptor neurons to elicit pain via TLR7 (Park et al. 2014). It is also possible that extracellular miRNAs released from central primary afferents may activate microglia through TLR7. It has been reported that miRNA let-7b induces TNFα release from brain microglia via TLR7 (Lehmann et al. 2012). Furthermore, transcriptome profiles revealed the distinctive difference in their functional phenotypes between early and late phase microglia even though they are difficult to distinguish by morphology alone (Fig. 1B).

3. Role of microglial miR-29c in initiation/development of neuropathic pain

I chose ATP as a microglia activator in vitro culture system.

Although there are many known microglia activators such as lipopolysaccharide (LPS) and lipid molecules, we used the background information that P2X and P2Y signals are quite critical for pain hypersensitivity after peripheral nerve injury, which is stressed in a previous report (Tsuda et al. 2003; Kobayashi et al. 2008). Indeed, it has been demonstrated that intrathecal injection of ATP-activated microglia produces mechanical hypersensitivity (Tsuda et al. 2003), and activation of P2Y12 receptor by released ATP or the hydrolyzed products activate p38 MAPK pathway and may play a crucial role in the generation of neuropathic pain (Kobayashi et al. 2008). While LPS has been used as a classic activating agent to stimulate microglia (Nakamura et al. 1999), LPS is an exogenous substance as the major component of the outer membrane of a gram-negative bacterial cell wall and is not directly associated with neuropathic pain following peripheral nerve injury. Thus, functional properties of LPS-activated microglia could be different from those of ATP-activated microglia (Nakamura et al. 1999).

I observed that down-regulation of miR-29c might be involved in initial pain response. From in vitro microglial culture experiments with cytokine profiling and pp38 analysis, I verified that miR-29c inhibition recapitulates the profile of activated microglia and TNFα could be

downstream of the pathway targeted by miR-29c. Furthermore, behavioral studies in mouse revealed down-regulation of miR-29c in early POD1 spinal microglia following nerve injury modulates pain response, which may recapitulate initiation/development of neuropathic pain. Growing body of evidence indicate that miRNAs have a substantial role in modulating complicated pain pathways (Bhalala et al. 2013; Lutz et al. 2014; Pan et al. 2014; Park et al. 2014; von Schack et al. 2011). Furthermore, a recent study also demonstrated that the level of miR-29c is decreased in the serum of complex regional pain syndrome patients (McDonald et al. 2014), suggesting potential role of miR-29c in chronic pain. Given that Gria1 might not be a downstream target of miR-29c (Fig. 8D), further work is required to identify target genes regulated by miR-29c and how those genes have functional significance in the neuropathic pain conditions.

4. Individual heterogeneity of spinal microglia in transcriptome

Like individual cells found in other tissues (Lawson et al. 1990), spinal microglia displayed substantial estimated individual variation in their transcriptome. Measurement of variation is not as sensitive as single cell measurements due to fact this thesis necessitated the pooling of 10 cells for

the high-resolution transcriptome analysis. Under random sampling, the variance of the mean of the samples is expected to be proportional to the variance of the individual cells. Nevertheless, I note that pooled cell measurements are indirect estimates of individual variation. I hypothesized that individual microglia in their normal state might exhibit heterogeneous gene expression to dynamically reflect microenvironmental changes. However, external stimuli such as skin lesion may lead to transient coordinated expression of gene, which may relax back into natural cell-to-cell heterogeneity. In the late phase of injury, under the continuous stimuli from the injured nerves, certain specific set of gene may remain coordinately expressed, leading to reduced variability in that gene set and functionally associated with the patho-physiological neuropathic pain outcome. Thus, examination of single-cell level variability may be a powerful tool in identifying novel key genes under specific stimulus.

5. Role of microglial Gria1 in maintenance of neuropathic pain

Since previous studies have mostly focused on the up-regulated genes after nerve injury (Griffin et al. 2007; Strong et al. 2012), most of the 56 genes identified with variation analysis in this study were rarely detected

from such whole tissue expression profiling. From these genes I focused on Gria1 as a strong candidate gene for functional role and knockdown of microglial Gria1 produced mechanical allodynia in naïve mice, which was reversed by TNFα inhibitor (Fig. 9F). Previous studies demonstrated that expression of Gria1 is significantly decreased in activated brain microglia and unexpectedly, potentiating microglial AMPA receptors by AMPA receptor agonist inhibits TNFα release, whereas activation of AMPA receptor by glutamate promotes release of TNF by rat microglia (Hagino et al. 2004). In this study, I found that the down-regulation of microglial GluR1 may lead to increased TNFα release (Pocock and Kettenmann 2007) contributing to central sensitization in the spinal cord that might lead to the maintenance of neuropathic pain. It was found that both miR-29c and Gria1 were also highly expressed in neurons in the spinal cord (Fig. 10B) such that the strong signals from the neurons made it difficult to determine their levels in microglia. However, I believe this does not affect the hypothesis that miR-29c and Gria 1 are involved in microglial regulation as the functional role of the genes may be cell-type-specific. Indeed, it is notable that I clearly observed down-regulation of miR-29c in the spinal dorsal horn after nerve injury (Fig. 10A) as well as in the original transcriptome data.

In summary, this study demonstrates that transcriptome analysis

with individual collections of spinal microglia can be a relevant tool to reveal a microglial gene-expression signature following peripheral nerve injury. Although transcriptome analysis of single-cell is not as simple as whole tissue or cell population analysis, cell-to-cell variation and changes in this variation in response to stimulus can be used to identify components of an elusive pathway. However, it does not mean that such an approach is highly specific or sensitive. Rather, it is more likely to yield targets genes that are difficult to be found by other approaches (Clyne et al. 1999). This high-resolution analysis reveals significant difference in gene profile between early (POD1) and late (POD7) microglia and it is likely that microglia exhibits functionally distinctive phenotypic changes over time following nerve injury. Of note, down-regulation of miR-29c in early spinal microglia following peripheral nerve injury might be important for the initiation/development of neuropathic pain, and Gria1 for the maintenance of neuropathic pain. This work provides insight into spinal microglia biology and potential new microglia targets for the treatment of chronic pain such as neuropathic pain.

REFERENCES

Abbadie C. 2005. Chemokines, chemokine receptors and pain. Trends Immunol. 26(10):529-534.

Beggs S, Trang T, Salter MW. 2012. P2x4r+ microglia drive neuropathic pain. Nat Neurosci. 15(8):1068-1073.

Berta T, Park CK, Xu ZZ, Xie RG, Liu T, Lu N, Liu YC, Ji RR. 2014. Extracellular caspase-6 drives murine inflammatory pain via microglial tnf-alpha secretion. J Clin Invest. 124(3):1173-1186.

Bettoni I, Comelli F, Rossini C, Granucci F, Giagnoni G, Peri F, Costa B. 2008. Glial tlr4 receptor as new target to treat neuropathic pain: Efficacy of a new receptor antagonist in a model of peripheral nerve injury in mice. Glia. 56(12):1312-1319.

Bhalala OG, Srikanth M, Kessler JA. 2013. The emerging roles of microrna s in cns injuries. Nat Rev Neurol. 9(6):328-339.

Block ML, Zecca L, Hong JS. 2007. Microglia-mediated neurotoxicity: Uncovering the molecular mechanisms. Nat Rev Neurosci. 8(1):57-69.

Butovsky O, Jedrychowski MP, Moore CS, Cialic R, Lanser AJ, Gabriely G, Koeglsperger T, Dake B, Wu PM, Doykan CE et al. 2014. Identification

of a unique tgf-beta-dependent molecular and functional signature in microglia. Nat Neurosci. 17(1):131-143.

Calvo M, Bennett DL. 2012. The mechanisms of microgliosis and pain following peripheral nerve injury. Exp Neurol. 234(2):271-282.

Campbell JN, Meyer RA. 2006. Mechanisms of neuropathic pain. Neuron. 52(1):77-92.

Cardona AE, Pioro EP, Sasse ME, Kostenko V, Cardona SM, Dijkstra IM, Huang D, Kidd G, Dombrowski S, Dutta R et al. 2006. Control of microglial neurotoxicity by the fractalkine receptor. Nat Neurosci. 9(7):917-924.

Chaplan SR, Bach FW, Pogrel JW, Chung JM, Yaksh TL. 1994. Quantitative assessment of tactile allodynia in the rat paw. J Neurosci Methods. 53(1):55-63.

Chiu IM, Barrett LB, Williams EK, Strochlic DE, Lee S, Weyer AD, Lou S, Bryman GS, Roberson DP, Ghasemlou N et al. 2014. Transcriptional profiling at whole population and single cell levels reveals somatosensory neuron molecular diversity. Elife. 3.

Chiu IM, Morimoto ET, Goodarzi H, Liao JT, O'Keeffe S, Phatnani HP, Muratet M, Carroll MC, Levy S, Tavazoie S et al. 2013. A neurodegeneration-specific gene-expression signature of acutely isolated microglia from an amyotrophic lateral sclerosis mouse model. Cell reports. 4(2):385-401.

Clark AK, Yip PK, Grist J, Gentry C, Staniland AA, Marchand F, Dehvari M, Wotherspoon G, Winter J, Ullah J et al. 2007. Inhibition of spinal microglial cathepsin s for the reversal of neuropathic pain. Proc Natl Acad Sci U S A. 104(25):10655-10660.

Clyne PJ, Warr CG, Freeman MR, Lessing D, Kim J, Carlson JR. 1999. A novel family of divergent seven-transmembrane proteins: Candidate odorant receptors in drosophila. Neuron. 22(2):327-338.

Costigan M, Belfer I, Griffin RS, Dai F, Barrett LB, Coppola G, Wu T, Kiselycznyk C, Poddar M, Lu Y et al. 2010. Multiple chronic pain states are associated with a common amino acid-changing allele in kcns1. Brain : a journal of neurology. 133(9):2519-2527.

Costigan M, Scholz J, Woolf CJ. 2009. Neuropathic pain: A maladaptive response of the nervous system to damage. Annu Rev Neurosci. 32:1-32.

Coull JA, Beggs S, Boudreau D, Boivin D, Tsuda M, Inoue K, Gravel C, Salter MW, De Koninck Y. 2005. Bdnf from microglia causes the shift in neuronal anion gradient underlying neuropathic pain. Nature. 438(7070):1017-1021.

DeLeo JA, Rutkowski MD, Stalder AK, Campbell IL. 2000. Transgenic expression of tnf by astrocytes increases mechanical allodynia in a mouse neuropathy model. Neuroreport. 11(3):599-602.

Del Rı´o-Hortega P. 1919. El tercer elemento de los centros nerviosos. Bol Soc Esp Biol. 9:69-120.

Dixon WJ. 1980. Efficient analysis of experimental observations. Annual review of pharmacology and toxicology. 20:441-462.

Dueck H, Eberwine J, Kim J. 2016. Variation is function: Are single cell differences functionally important?: Testing the hypothesis that single cell variation is required for aggregate function. Bioessays. 38(2):172-180.

Dworkin RH, Backonja M, Rowbotham MC, Allen RR, Argoff CR, Bennett GJ, Bushnell MC, Farrar JT, Galer BS, Haythornthwaite JA et al. 2003. Advances in neuropathic pain: Diagnosis, mechanisms, and treatment recommendations. Arch Neurol. 60(11):1524-1534.

Eberwine J, Sul JY, Bartfai T, Kim J. 2014. The promise of single-cell sequencing. Nature methods. 11(1):25-27.

Esumi S, Wu SX, Yanagawa Y, Obata K, Sugimoto Y, Tamamaki N. 2008. Method for single-cell microarray analysis and application to gene-expression profiling of gabaergic neuron progenitors. Neurosci Res. 60(4):439-451.

Gao YJ, Ji RR. 2010. Chemokines, neuronal-glial interactions, and central processing of neuropathic pain. Pharmacol Ther. 126(1):56-68.

Giordan M. 2013. A two-stage procedure for the removal of batch effects in microarray studies. Statistics in Biosciences. 6(1): 73-84.

Grace PM, Hutchinson MR, Maier SF, Watkins LR. 2014. Pathological pain and the neuroimmune interface. Nature reviews Immunology. 14(4):217-231.

Graeber MB, Streit WJ. 2010. Microglia: Biology and pathology. Acta Neuropathol. 119(1):89-105.

Griffin RS, Costigan M, Brenner GJ, Ma CHE, Scholz J, Moss A, Allchorne AJ, Stahl GL, Woolf CJ. 2007. Complement induction in spinal cord

microglia results in anaphylatoxin c5a-mediated pain hypersensitivity. Journal of Neuroscience. 27(32):8699-8708.

Hagino Y, Kariura Y, Manago Y, Amano T, Wang B, Sekiguchi M, Nishikawa K, Aoki S, Wada K, Noda M. 2004. Heterogeneity and potentiation of ampa type of glutamate receptors in rat cultured microglia. Glia. 47(1):68-77.

Hains BC, Waxman SG. 2006. Activated microglia contribute to the maintenance of chronic pain after spinal cord injury. J Neurosci. 26:4308-4317.

Hanisch UK, Kettenmann H. 2007. Microglia: Active sensor and versatile effector cells in the normal and pathologic brain. Nat Neurosci. 10(11):1387-1394.

Hathway GJ, Vega-Avelaira D, Moss A, Ingram R, Fitzgerald M. 2009. Brief, low frequency stimulation of rat peripheral c-fibres evokes prolonged microglial-induced central sensitization in adults but not in neonates. Pain. 144(1-2):110-118.

Haynes SE, Hollopeter G, Yang G, Kurpius D, Dailey ME, Gan WB, Julius D. 2006. The p2y12 receptor regulates microglial activation by extracellular nucleotides. Nat Neurosci. 9:1512-1519.

Hickman SE, Kingery ND, Ohsumi TK, Borowsky ML, Wang LC, Means TK, El Khoury J. 2013. The microglial sensome revealed by direct rna sequencing. Nat Neurosci. 16(12):1896-1905.

Hylden JL, Wilcox GL. 1980. Intrathecal morphine in mice: A new technique. Eur J Pharmacol. 67(2-3):313-316.

Inoue K, Tsuda M. 2009. Microglia and neuropathic pain. Glia. 57(14):1469-1479.

Irizarry RA, Bolstad BM, Collin F, Cope LM, Hobbs B, Speed TP. 2003. Summaries of affymetrix genechip probe level data. Nucleic acids research. 31(4):e15.

Ji RR, Suter MR. 2007. P38 mapk, microglial signaling, and neuropathic pain. Mol Pain. 3:33.

Jin SX, Zhuang ZY, Woolf CJ, Ji RR. 2003. P38 mitogen-activated protein kinase is activated after a spinal nerve ligation in spinal cord microglia and dorsal root ganglion neurons and contributes to the generation of neuropathic pain. J Neurosci. 23(10):4017-4022.

Jung S, Aliberti J, Graemmel P, Sunshine MJ, Kreutzberg GW, Sher A, Littman DR. 2000. Analysis of fractalkine receptor cx(3)cr1 function by

targeted deletion and green fluorescent protein reporter gene insertion. Molecular and cellular biology. 20(11):4106-4114.

Kettenmann H, Hanisch UK, Noda M, Verkhratsky A. 2011. Physiology of microglia. Physiol Rev. 91(2):461-553.

Kim D, Kim MA, Cho IH, Kim MS, Lee S, Jo EK, Choi SY, Park K, Kim JS, Akira S et al. 2007. A critical role of toll-like receptor 2 in nerve injury-induced spinal cord glial cell activation and pain hypersensitivity. J Biol Chem. 282(20):14975-14983.

Kim SH, Chung JM. 1992. An experimental model for peripheral neuropathy produced by segmental spinal nerve ligation in the rat. Pain. 50(3):355-363.

Kim YH, Back SK, Davies AJ, Jeong H, Jo HJ, Chung G, Na HS, Bae YC, Kim SJ, Kim JS et al. 2012. Trpv1 in gabaergic interneurons mediates neuropathic mechanical allodynia and disinhibition of the nociceptive circuitry in the spinal cord. Neuron. 74(4):640-647.

Kobayashi K, Yamanaka H, Fukuoka T, Dai Y, Obata K, Noguchi K. 2008. P2y12 receptor upregulation in activated microglia is a gateway of p38 signaling and neuropathic pain. J Neurosci. 28(11):2892-2902.

Kolodziejczyk AA, Kim JK, Svensson V, Marioni JC, Teichmann SA. 2015. The technology and biology of single-cell rna sequencing. Molecular cell. 58(4):610-620.

Kreutzberg GW. 1996. Microglia: A sensor for pathological events in the cns. Trends Neurosci. 19(8):312-318.

Lacroix-Fralish ML, Tawfik VL, Tanga FY, Spratt KF, DeLeo JA. 2006. Differential spinal cord gene expression in rodent models of radicular and neuropathic pain. Anesthesiology. 104(6):1283-1292.

Lawson LJ, Perry VH, Dri P, Gordon S. 1990. Heterogeneity in the distribution and morphology of microglia in the normal adult mouse brain. Neuroscience. 39(1):151-170.

Lee S, Varvel NH, Konerth ME, Xu G, Cardona AE, Ransohoff RM, Lamb BT. 2010. Cx3cr1 deficiency alters microglial activation and reduces beta-amyloid deposition in two alzheimer's disease mouse models. Am J Pathol. 177(5):2549-2562.

Lehmann SM, Kruger C, Park B, Derkow K, Rosenberger K, Baumgart J, Trimbuch T, Eom G, Hinz M, Kaul D et al. 2012. An unconventional role for mirna: Let-7 activates toll-like receptor 7 and causes neurodegeneration. Nat Neurosci. 15(6):827-835.

Livak KJ, Schmittgen TD. 2001. Analysis of relative gene expression data using real-time quantitative pcr and the 2(-delta delta c(t)) method. Methods. 25(4):402-408.

Lutz BM, Bekker A, Tao YX. 2014. Noncoding rnas: New players in chronic pain. Anesthesiology. 121(2):409-417.

Masuda T, Ozono Y, Mikuriya S, Kohro Y, Tozaki-Saitoh H, Iwatsuki K, Uneyama H, Ichikawa R, Salter MW, Tsuda M et al. 2016. Dorsal horn neurons release extracellular atp in a vnut-dependent manner that underlies neuropathic pain. Nat Commun. 7:12529.

McDonald MK, Tian Y, Qureshi RA, Gormley M, Ertel A, Gao R, Aradillas Lopez E, Alexander GM, Sacan A, Fortina P et al. 2014. Functional significance of macrophage-derived exosomes in inflammation and pain. Pain.

Mika J, Zychowska M, Popiolek-Barczyk K, Rojewska E, Przewlocka B. 2013. Importance of glial activation in neuropathic pain. European journal of pharmacology. 716(1-3):106-119.

Mittelbronn M, Dietz K, Schluesener HJ, Meyermann R. 2001. Local distribution of microglia in the normal adult human central nervous

system differs by up to one order of magnitude. Acta Neuropathol. 101(3):249-255.

Nakamura Y, Si QS, Kataoka K. 1999. Lipopolysaccharide-induced microglial activation in culture: Temporal profiles of morphological change and release of cytokines and nitric oxide. Neurosci Res. 35(2):95-100.

Nikitin A, Egorov S, Daraselia N, Mazo I. 2003. Pathway studio--the analysis and navigation of molecular networks. Bioinformatics. 19(16):2155-2157.

Nimmerjahn A, Kirchhoff F, Helmchen F. 2005. Resting microglial cells are highly dynamic surveillants of brain parenchyma in vivo. Science. 308(5726):1314-1318.

Pan Z, Zhu LJ, Li YQ, Hao LY, Yin C, Yang JX, Guo Y, Zhang S, Hua L, Xue ZY et al. 2014. Epigenetic modification of spinal mir-219 expression regulates chronic inflammation pain by targeting camkiigamma. J Neurosci. 34(29):9476-9483.

Parakalan R, Jiang B, Nimmi B, Janani M, Jayapal M, Lu J, Tay SS, Ling EA, Dheen ST. 2012. Transcriptome analysis of amoeboid and ramified

microglia isolated from the corpus callosum of rat brain. BMC Neurosci. 13:64.

Park CK, Xu ZZ, Berta T, Han Q, Chen G, Liu XJ, Ji RR. 2014. Extracellular micrornas activate nociceptor neurons to elicit pain via tlr7 and trpa1. Neuron. 82(1):47-54.

Pocock JM, Kettenmann H. 2007. Neurotransmitter receptors on microglia. Trends Neurosci. 30(10):527-535.

Poulin JF, Zou J, Drouin-Ouellet J, Kim KY, Cicchetti F, Awatramani RB. 2014. Defining midbrain dopaminergic neuron diversity by single-cell gene expression profiling. Cell Rep. 9(3):930-943.

Raghavendra V, Tanga F, DeLeo JA. 2003. Inhibition of microglial activation attenuates the development but not existing hypersensitivity in a rat model of neuropathy. J Pharmacol Exp Ther. 306(2):624-630.

Ramesh G, MacLean AG, Philipp MT. 2013. Cytokines and chemokines at the crossroads of neuroinflammation, neurodegeneration, and neuropathic pain. Mediators Inflamm. 2013:480739.

Reeve AJ, Patel S, Fox A, Walker K, Urban L. 2000. Intrathecally administered endotoxin or cytokines produce allodynia, hyperalgesia

and changes in spinal cord neuronal responses to nociceptive stimuli in the rat. Eur J Pain. 4(3):247-257.

Ren K, Dubner R. 2010. Interactions between the immune and nervous systems in pain. Nat Med. 16(11):1267-1276.

Salter MW, Beggs S. 2014. Sublime microglia: Expanding roles for the guardians of the cns. Cell. 158(1):15-24.

Sandberg R. 2014. Entering the era of single-cell transcriptomics in biology and medicine. Nature methods. 11(1):22-24.

Sayed D, Abdellatif M. 2011. Micrornas in development and disease. Physiological reviews. 91(3):827-887.

Schafers M, Geis C, Brors D, Yaksh TL, Sommer C. 2002. Anterograde transport of tumor necrosis factor-alpha in the intact and injured rat sciatic nerve. J Neurosci. 22(2):536-545

Schafers M, Svensson CI, Sommer C, Sorkin LS. 2003. Tumor necrosis factor-alpha induces mechanical allodynia after spinal nerve ligation by activation of p38 mapk in primary sensory neurons. J Neurosci. 23(7):2517-2521.

Scholz J, Woolf CJ. 2007. The neuropathic pain triad: Neurons, immune cells and glia. Nat Neurosci. 10(11):1361-1368.

Smith JA, Das A, Ray SK, Banik NL. 2012. Role of pro-inflammatory cytokines released from microglia in neurodegenerative diseases. Brain Res Bull. 87(1):10-20.

Sommer C, Lindenlaub T, Teuteberg P, Schafers M, Hartung T, Toyka KV. 2001a. Anti-tnf-neutralizing antibodies reduce pain-related behavior in two different mouse models of painful mononeuropathy. Brain Res. 913(1):86-89.

Sommer C, Schafers M, Marziniak M, Toyka KV. 2001b. Etanercept reduces hyperalgesia in experimental painful neuropathy. J Peripher Nerv Syst. Tsuda M, Mizokoshi A, Shigemoto-Mogami Y, Koizumi S, Inoue K. 2004. Activation of p38 mitogen-activated protein kinase in spinal hyperactive microglia contributes to pain hypersensitivity following peripheral nerve injury. Glia. 45(1):89-95.

6(2):67-72.

Streit WJ. 2002. Microglia as neuroprotective, immunocompetent cells of the cns. Glia. 40(2):133-139.

Strong JA, Xie W, Coyle DE, Zhang JM. 2012. Microarray analysis of rat sensory ganglia after local inflammation implicates novel cytokines in pain. PLoS One. 7(7):e40779.

Sung CS, Wen ZH, Chang WK, Ho ST, Tsai SK, Chang YC, Wong CS. 2004. Intrathecal interleukin-1beta administration induces thermal hyperalgesia by activating inducible nitric oxide synthase expression in the rat spinal cord. Brain Res. 1015(1-2):145-153.

Tanga FY, Nutile-McMenemy N, DeLeo JA. 2005. The cns role of toll-like receptor 4 in innate neuroimmunity and painful neuropathy. Proc Natl Acad Sci U S A. 102(16):5856-5861.

Tozaki-Saitoh H, Tsuda M, Miyata H, Ueda K, Kohsaka S, Inoue K. 2008. P2y12 receptors in spinal microglia are required for neuropathic pain after peripheral nerve injury. J Neurosci. 28:4949-4956.

Tsuda M, Inoue K, Salter MW. 2005. Neuropathic pain and spinal microglia: A big problem from molecules in "small" glia. Trends Neurosci. 28(2):101-107.

Tsuda M, Shigemoto-Mogami Y, Koizumi S, Mizokoshi A, Kohsaka S, Salter MW, Inoue K. 2003. P2x4 receptors induced in spinal microglia gate tactile allodynia after nerve injury. Nature. 424(6950):778-783.

Ulmann L, Hatcher JP, Hughes JP, Chaumont S, Green PJ, Conquet F, Buell GN, Reeve AJ, Chessell IP, Rassendren F. 2008. Up-regulation of p2x4 receptors in spinal microglia after peripheral nerve injury mediates bdnf release and neuropathic pain. J Neurosci. 28:11263-11268.

Usoskin D, Furlan A, Islam S, Abdo H, Lonnerberg P, Lou D, Hjerling-Leffler J, Haeggstrom J, Kharchenko O, Kharchenko PV et al. 2015. Unbiased classification of sensory neuron types by large-scale single-cell rna sequencing. Nat Neurosci. 18(1):145-153.

Vicuna L, Strochlic DE, Latremoliere A, Bali KK, Simonetti M, Husainie D, Prokosch S, Riva P, Griffin RS, Njoo C et al. 2015. The serine protease inhibitor serpina3n attenuates neuropathic pain by inhibiting t cell-derived leukocyte elastase. Nat Med. 21(5):518-523.

von Schack D, Agostino MJ, Murray BS, Li Y, Reddy PS, Chen J, Choe SE, Strassle BW, Li C, Bates B et al. 2011. Dynamic changes in the microrna expression profile reveal multiple regulatory mechanisms in the spinal nerve ligation model of neuropathic pain. PLoS One. 6(3):e17670.

Watkins LR, Milligan ED, Maier SF. 2001. Glial activation: A driving force for pathological pain. Trends in Neurosciences. 24(8):450-455.

Woolf CJ. 2011. Central sensitization: Implications for the diagnosis and treatment of pain. Pain. 152(3 Suppl):S2-15.

Yang L, Zhang FX, Huang F, Lu YJ, Li GD, Bao L, Xiao HS, Zhang X. 2004. Peripheral nerve injury induces trans-synaptic modification of channels, receptors and signal pathways in rat dorsal spinal cord. Eur J Neurosci. 19(4):871-883.

Zhang JM, An J. 2007. Cytokines, inflammation, and pain. Int Anesthesiol Clin. 45(2):27-37.

Zhuang ZY, Kawasaki Y, Tan PH, Wen YR, Huang J, Ji RR. 2007. Role of the cx3cr1/p38 mapk pathway in spinal microglia for the development of neuropathic pain following nerve injury-induced cleavage of fractalkine. Brain, behavior, and immunity. 21(5):642-651.

국문초록

소교세포는 중추신경에 존재하는 면역세포로, 항상성을 유지하고 신경손상을 감지한다. 말초신경이 손상되면 중추신경에 존재하는 소교세포가 활성화되는데 이러한 소교세포의 활성화는 중추신경 과민화를 통한 통증과민증 유발에 중요하다고 알려져 있다. 활성화된 소교세포는 형태학적으로 비대하게 변하며, 과도한 증식, 싸이토카인 등 염증물질의 분비 및 여러가지 유전자 발현의 변화를 수반한다. 통증관련 유전자를 찾기 위해 척수 신경절이나 척수와 같은 조직 수준에서의 대규모 스크리닝 연구가 이루어졌고 이를 통해 통증과 관련된 다양한 유전자의 발현 변화가 밝혀졌다. 그러나, 이러한 유전자의 변화는 대부분 소교세포가 아닌 신경세포에서 일어나는 발현 변화였으며 이는, 여러 타입의 세포가 섞여있는 척수와 같은 조직 전체의 전사체에서 상대적으로 조직의 적은 부분을 차지하는 소교세포와 같은 세포타입 특이적인 발현 변화를 확인하는 것이 한계가 있음을 나타낸다.

따라서 이번 연구에서 본 연구자는 $Cx3cr1^{+/GFP}$ 마우스를

사용하여 각 각의 소교세포 10개를 하나의 샘플로 수집하는 고해상도의 전사체 분석법을 통하여 말초신경 손상 후 소교세포가 활성화되는 동안 소교세포 특이적인 유전자의 발현 변화를 알아보았다. 차별적으로 분석된 유전자 (DEGs) 분석에서, miR-29c가 소교세포 활성화 및 수술 후 1일째 신경병증성 통증의 발병에 중요한 요소임을 확인할 수 있었다. 신경손상 후 1일째인 초기의 소교세포는 손상 후 7일째의 후기 소교세포와 비교할 때 상당히 다른 발현 프로파일을 나타냈으며, 이러한 결과는 신경병증성 통증의 발달단계에서 유지단계로의 전이와 관련있을 것으로 보여진다. 또한, 발현의 변이분석을 통해 신경병증성 통증의 유지단계와 관련이 있을 수 있는 Gria1을 포함한 유전자 56개의 소교세포 유전자를 밝혔다. 이 연구를 통해 본 연구자는 척수 소교세포의 생물학에 대한 통찰을 제공하고 신경병증성 통증 치료를 위한 새로운 소교세포의 타깃을 제시하였다.

주요어: 척수 소교세포, 소교세포 활성화, 고해상도 전사체,

신경병증성 통증, MiR-29c, Gria1

학번: 2010-30656